frontiers | Frontiers in Earth Science

ORIGINAL RESEARCH
published: 30 June 2022
doi: 10.3389/feart.2022.837354

# Deformation Styles and Multi-Stage Evolution History of a Large Intraplate Strike-Slip Fault System in a Paleozoic Superimposed Basin: A Case Study From the Tarim Basin, NW China

*Yuan Neng*[1,2]*, *Yong Li*[3], *Jiafu Qi*[1,2], *Xiao Ma*[1,2]*, *Liang Zuo*[1,2] and *Ping Chen*[1,2]

[1]Department of Petroleum, China University of Petroleum–Beijing at Karamay, Karamay, China, [2]State Key Laboratory of Petroleum Resources and Prospecting, China University of Petroleum, Beijing, China, [3]Research Institute of Petroleum Exploration and Development, Tarim Oilfield Company, PetroChina, Korla, China

The complex deformation styles of large intraplate strike-slip fault systems in the multi-stage superimposed basin are hot topics worldwide. This article proposes structural models and evolution processes for such strike-slip fault systems in the Tarim Basin based on high-resolution 3D seismic data and deep wells. Our analyses reveal that strike-slip fault in the Tarim Basin formed with different structural styles in five tectonic layers from the Sinian to the Permian that accompanies the Sinian rift systems and uplift, the Lower–Middle Cambrian reversed faults and salt tectonics, the Ordovician fault-karst systems, the Silurian to the Carboniferous en-echelon transtensional faults, and the Permian volcanic structures. Influenced by the multi-tectonic layers and complex evolution history, the strike-slip faults performed as multi-layer flower structures and various fault types. The evolution history of paleo-uplifts also influenced the distribution characteristics of strike-slip faults, such as X, diamond, and V shapes in the Tabei uplift and T shapes in the Tazhong uplift. The strike-slip faults formed in late Cambrian stage were associated with unconformities, inverted structures, and growth strata in deep layers. The different tectonic evolution models of the Tabei and the Tazhong uplift were built, which shows pre-existing structures, the lithological combinations from the rift basin to the marine basin, and the change of regional tectonic stress from the Cambrian to Permian are controlling factors of the strike-slip fault systems. These models provide a new interpretation method for intraplate strike-slip fault systems worldwide.

**Keywords: strike-slip fault system, deformation styles, ultra-deep layers, multi-stage evolution history, Tarim Basin**

OPEN ACCESS

***Edited by:***
*Shengji Wei,*
*Nanyang Technological University, Singapore*

***Reviewed by:***
*Shang Deng,*
*SINOPEC Petroleum Exploration and Production Research Institute, China*
*Andres Folguera,*
*University of Buenos Aires, Argentina*

***Correspondence:**
*Xiao Ma*
*2021592105@cupk.edu.cn*
*Yuan Neng*
*nengyuan@foxmail.com*

***Specialty section:***
*This article was submitted to Structural Geology and Tectonics, a section of the journal Frontiers in Earth Science*

***Received:*** *16 December 2021*
***Accepted:*** *17 May 2022*
***Published:*** *30 June 2022*

***Citation:***
*Neng Y, Li Y, Qi J, Ma X, Zuo L and Chen P (2022) Deformation Styles and Multi-Stage Evolution History of a Large Intraplate Strike-Slip Fault System in a Paleozoic Superimposed Basin: A Case Study From the Tarim Basin, NW China. Front. Earth Sci. 10:837354. doi: 10.3389/feart.2022.837354*

## 1 INTRODUCTION

The intraplate strike-slip fault system has been documented in detail by field studies (Woodcock and Fischer, 1986; Cunningham et al., 1996; Pluhar et al., 2006; Faulkner et al., 2003), seismic interpretation (Harding, 1974; Nicholson et al., 1986; Wu et al., 2020a; Deng et al., 2019), and analog experiment (Basile and Brun, 1999; Mcclay and Bonora, 2001; Dooley and Schreurs, 2012). Most strike-slip faults have experienced several evolution stages from initial fractures to large fault zones with complex structural patterns and internal architectures such as stepovers,

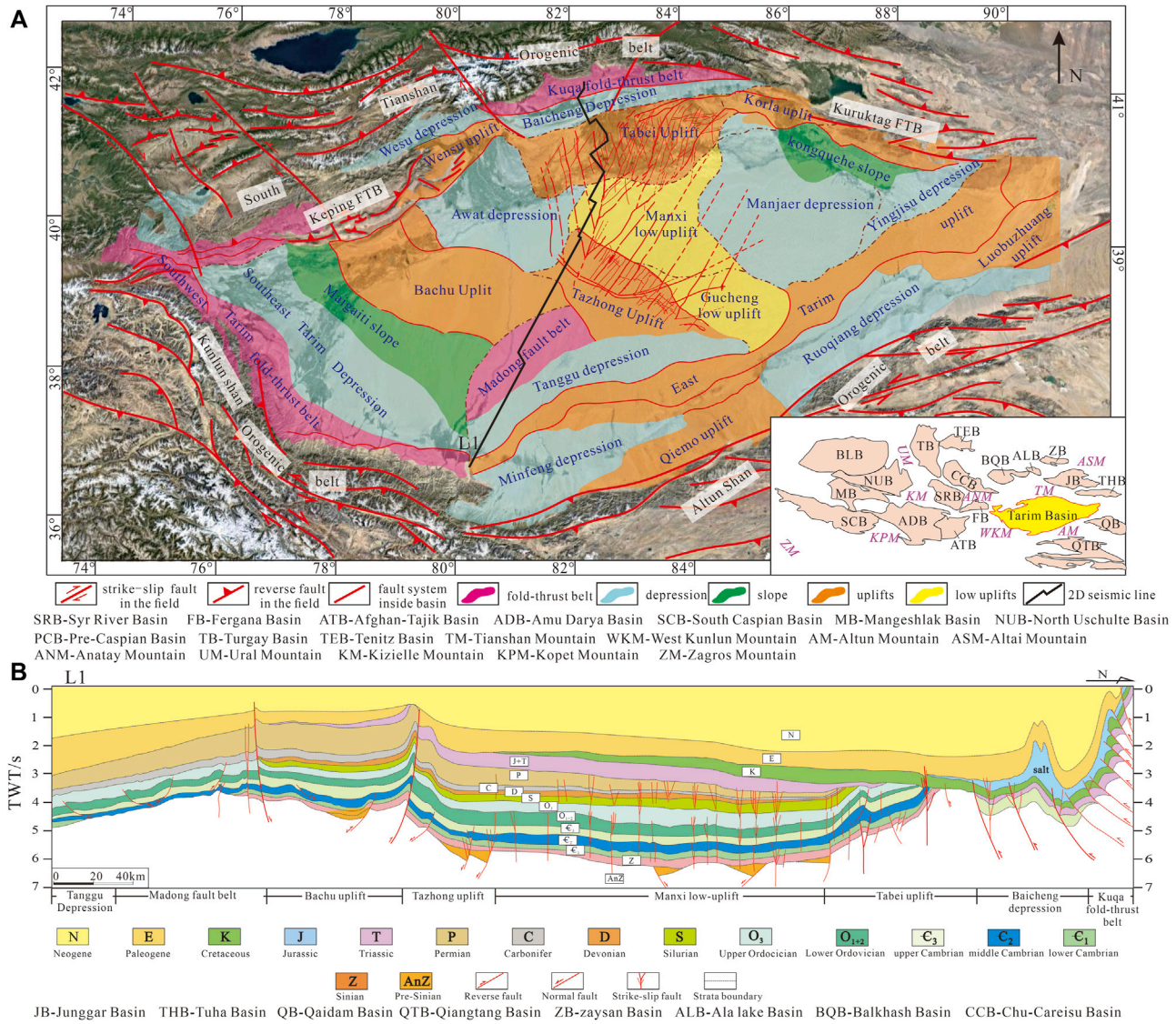


**FIGURE 1 | (A)** Geological map of the Tarim Basin (modified from Laborde et al., 2019). It is surrounded by the Tian Shan, Kunlun Shan, and Altun Shan Orogenic belts. Thrusts and strike-slip fault systems were found in the mountain belts. **(B)** Regional profile of the Tarim Basin (L1 line in **Figure 1**).

fault ramps, overlap zones, and secondary fault systems (Sylvester, 1988; Little, 1995; Aydin and Berryman, 2010). Some are caused by pre-existing structures such as paleo-continental plate boundaries as transform faults and trench-linked and indent-linked strike-slip faults due to the complex evolution history of the plate boundaries (Woodcock and Fischer, 1986; Storti et al., 2003). Others have initiated from earlier basin discontinuities such as basement thrusts, normal faults, block boundaries, and regional joints or fracture systems (Nur et al., 1986; Davis et al., 2000; Storti et al., 2003; Berglar et al., 2010). The change of the regional tectonic stress field and basin structural evolution history also have a significant effect on fault patterns. If basins experienced long and complex evolution histories, zones of pre-existing structures could be reactivated many times (Sutton and Waston, 1986; Storti et al., 2003; Rolland et al., 2013). The presence of a weak body, such as a thick salt layer, mud layer, and volcanic layer, along a developing strike-slip fault zone has a profound influence on patterns of strike-slip fault in vertical and map view (Zouaghi et al., 2005; Mathieu and Vries., 2011; Dooley and Schreurs, 2012). The strike-slip faults also influenced the locations, architectures, and subsidence histories of associated sedimentary basins, many of which are rich in hydrocarbons (Morley, 2002; Storti et al., 2003).

A large strike-slip fault system was distributed widely in the Paleozoic carbonate and clastic rock layers in the Tarim Basin (**Figure 1A**). The geometry, kinematics, and dynamics of such intraplate strike-slip fault systems become a research focus, since these characteristics of the strike-slip fault systems were evidence to investigate the long plate

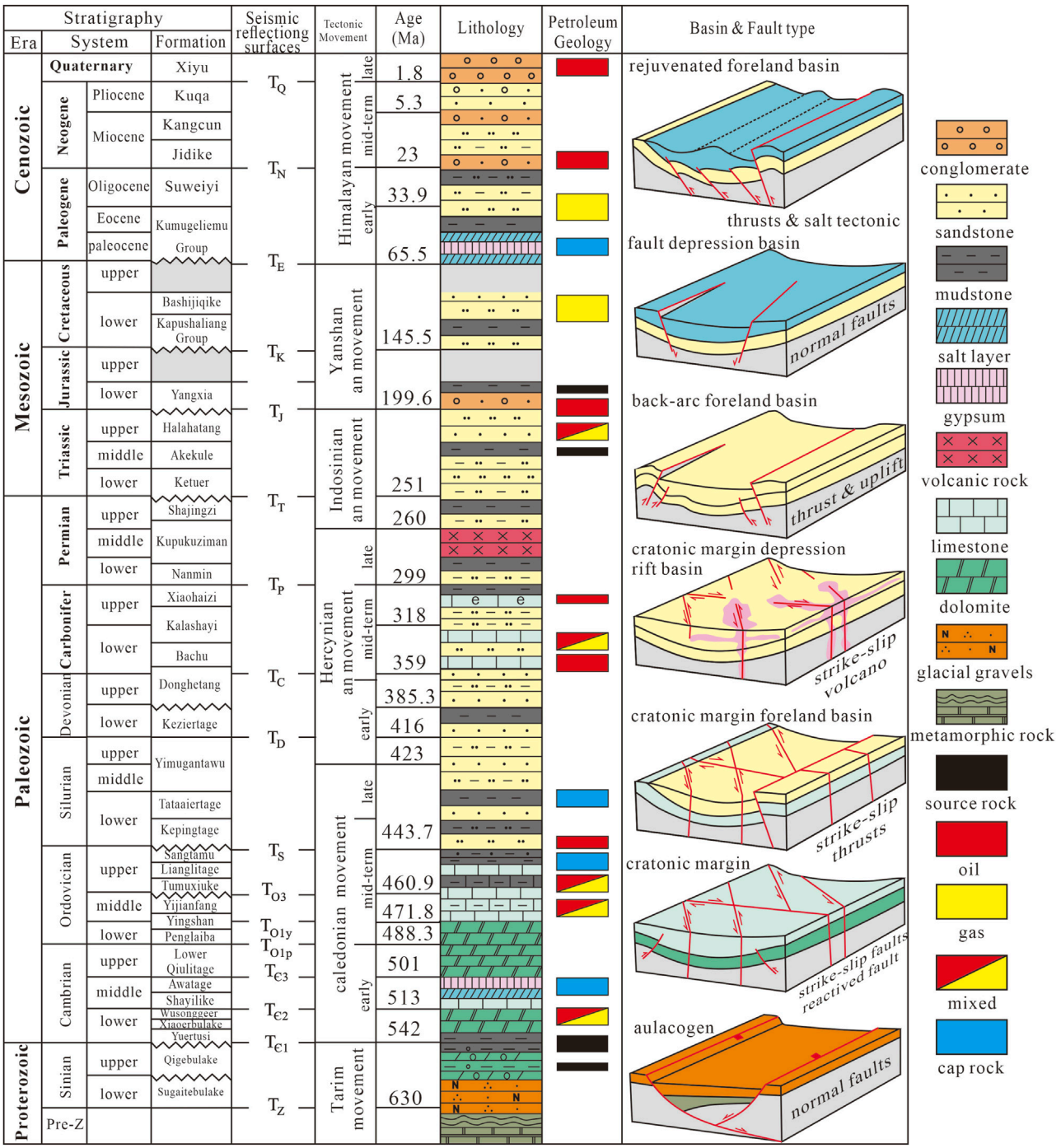


**FIGURE 2 |** Stratigraphical chart of the Tarim Basin. Seismic data reflecting surfaces, tectonic movements, petroleum geology, basin, and fault types in different periods are shown (modified from Yu et al., 2014; Deng et al., 2019).

tectonic movement history of north-western China (Jia et al., 1998; Li et al., 2012; Han et al., 2017; Neng et al., 2018; Wu et al., 2018; Deng et al., 2019; Wu et al., 2020a; Wu et al., 2020b; Deng et al., 2021). The Tarim Basin is characterized as a superimposed basin, which consists of rift systems, salt tectonics, thrust fault systems, paleo-uplifts, and strike-slip fault systems in sequence in a long and complicated evolution history spanning from the Precambrian to the Quaternary (**Figures 1B**, **2**) (Carroll et al., 1995; Li et al., 2013a; Lin et al., 2015; Neng et al., 2016), due to micro-craton breakup from

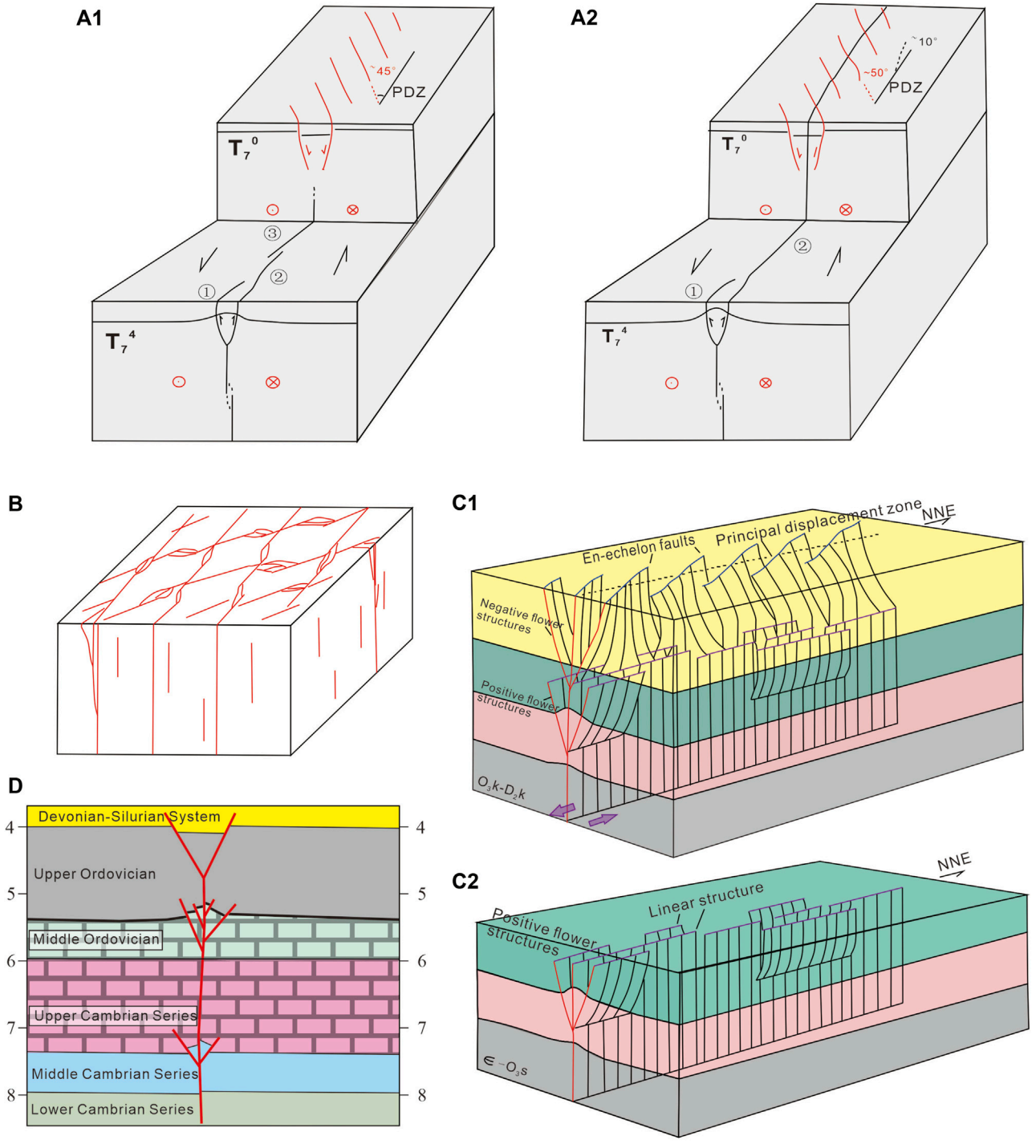


**FIGURE 3 |** Models of strike-slip faults in the central Tarim Basin of the previous research (modified from Han et al., 2017; Wu et al., 2020a; Deng et al., 2019): **(A1–A2)** models of the evolution history of strike-slip faults from the Manxi low uplift (modified from Deng et al., 2019), **(B)** model of strike-slip faults from the Tabei uplift (modified from Wu et al., 2020b), **(C1–C2)** models of the stages of evolution of strike-slip faults from the northern slope of the Tazhong uplift (modified from Han et al., 2017), and **(D)** model of strike-slip fault from the Tazhong uplift (modified from Neng et al., 2018).

Rodinia and re-matched together from the Caledonian Movement to the Himalayan Movement (Jia and Wei, 2002; Wu et al., 2018). High-resolution 2D/3D seismic data and deep wells have revealed details of the large strike-slip fault systems, ranging from the Tabei uplift to the Tazhong uplift (**Figure 1A**).

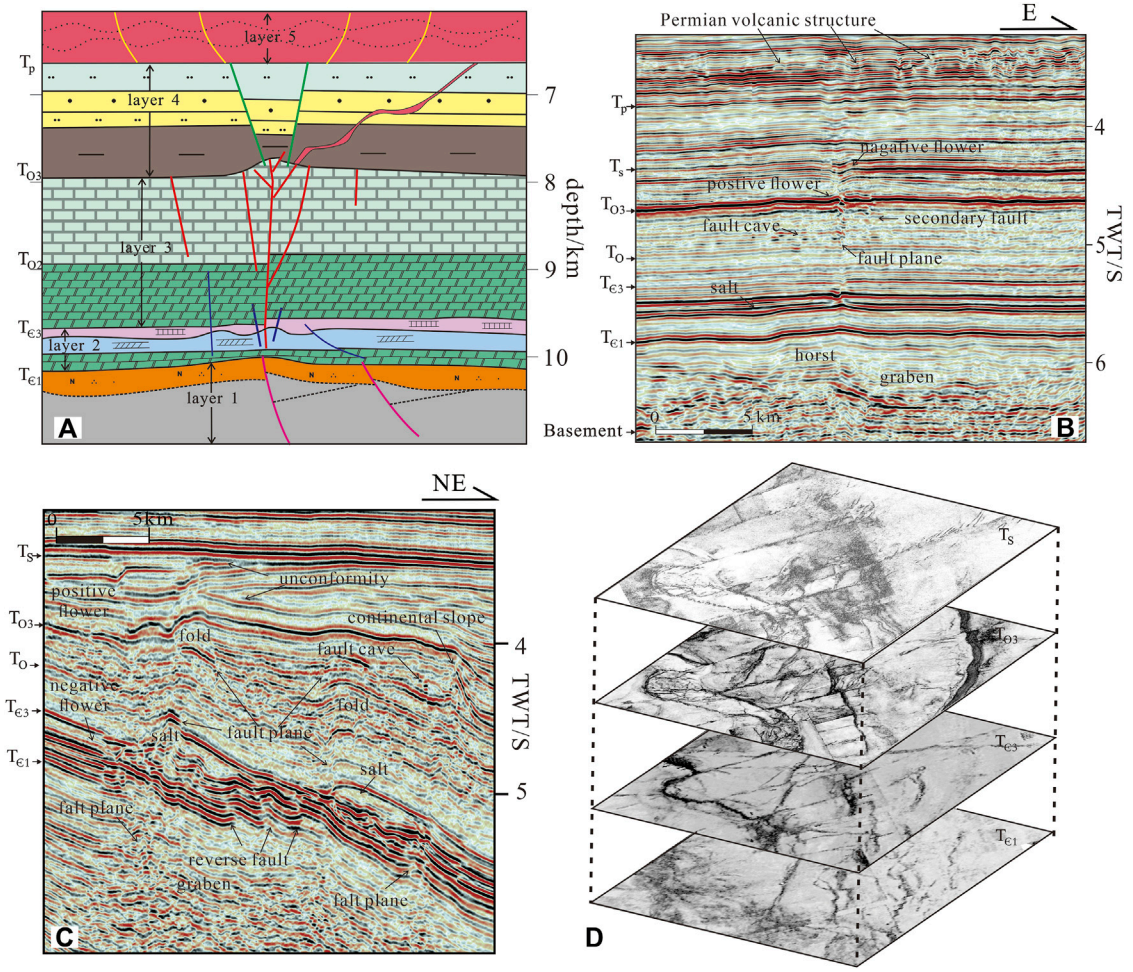


**FIGURE 4 |** Models of the strike-slip fault and typical seismic profiles and coherency cube slices of the main reflecting surface: **(A)** five-layer strike-slip fault model, **(B)** typical seismic profiles of the Manxi low uplift, **(C)** typical seismic profiles of the Tazhong uplift, and **(D)** coherency cube slice of the main reflecting surface of the Tazhong uplift.

Past research has focused on the distributions and characteristics of strike-slip fault systems and developed a basic framework for them (**Figure 3**). The strike-slip faults can be divided into three types: positive flower structures, negative flower structures, and liner shear structures (Wu et al., 2020a; Deng et al., 2019; Han et al., 2017, Deng et al., 2021). In map view, strike-slip faults also occur in linear, oblique, feather, en-echelon faults, conjugated faults, and horsetail types. The strike-slip fault formed different types in the Tabei and Tazhong uplift, which performed like X, diamond, V shapes in the Tabei uplift and Tshapes in the Tazhong uplift based on the combination style (Neng et al., 2018b; Wu et al., 2020a) (**Figure 1A**). The X-type fault represents that two groups of faults with different strikes cut each other, and the angle between the two faults is between 30 and 45°, The diamond-type fault is composed of two groups of the X-type faults, and the plane pattern presents a diamond shape in map view. The V-type fault is half of the X-type fault. The Y-type fault is composed of a main fault and branch faults, which is Y shaped on the plane. The T-type fault represents that two groups of faults with different strike cut each other, and the angle between the two faults is between 60 and 90°. The criterion of the fault-type determination and the supplementary coherency attribute maps are given in **Figure 8G**. Most current research has focused on the deformation of strike-slip faults on top of the Ordovician carbonate layers and younger layers above them (Yuzhu and Zhihong, 1996; Pang et al., 2013; Zhiqian and Tailiang, 2015; Yu et al., 2016; Lu et al., 2017; Shen et al., 2019; Haijun et al., 2020; Wang et al., 2020, **Figures 3A–C**). The influence on strike-slip fault by pre-existing structures and multi-stage evolution histories was also discussed from the Middle Ordovician to Permian (Wu et al., 2020b; Deng et al., 2019; Deng et al., 2022; Han et al., 2017), but research on the relationship between the strike-slip fault system and Sinian rift system, the Middle Cambrian evaporite rock layers, and the Permian volcanic structure is insufficient. Latest studies (Deng et al., 2022) have shed light on contrasting characteristics and

formation mechanisms of the two strike-slip faults in the Tabei and the Tazhong uplift, still proposing a distinct evolution model for the strike-slip faults of these two uplifts is essential to enhance the understanding of the coupling effect between the strike-slip fault evolution history and surrounding plate tectonic movements. Evidence from recently acquired 3D seismic data shows that some deformations within strike-slip fault belts are distributed in the Lower Cambrian and the Sinian tectonic layers (**Figure 4**). These structures are various between the Tabei uplift and Tazhong uplift, which are key to understanding the evolution history of strike-slip faults and the change of regional stress field. This paper applied recently acquired 3D seismic data from the Tabei uplift and Tazhong uplift to reveal the various deformation styles of strike-slip fault systems in different tectonic backgrounds. Structural models were also built for 3D seismic interpretation. The main aims of this study are 1) to build the models of strike-slip faults in different tectonic layers with other structures from the Sinian to the Permian, 2) to explain the formation mechanism of different types of faults in the Tabei uplift and Tazhong uplift, and 3) to provide new evolution models for the intraplate strike-slip fault system in the central Tarim Basin during the Paleozoic.

# 2 GEOLOGICAL SETTING

## 2.1 Tectonic Evolution History

The Tarim Basin is located in NW China. It is a typical superimposed basin that has experienced multi-stage evolution from the Neoproterozoic to the Quaternary closely related to the continental breakup and assemblage (Jia et al., 1998; Jia and Wei., 2002; Li et al., 2013a; Gao and Fan, 2014; Wu et al., 2018; Laborde et al., 2019; Qiu et al., 2019; Wu et al., 2020c; Qiu et al., 2022). This region encompasses an Archean-to-Early Neoproterozoic crystalline basement (Zhu et al., 2017; Wu et al., 2018) with very local distributed small rifts, which were trigged under the extension caused by the breakup of the Rodinia supercontinent. In Cambrian and Early Ordovician, the Tarim Basin was bounded by the South Tianshan Ocean to the north, North Altyn Ocean to the southeast, and Kudi Ocean to the southwest, respectively, and generally developed a succession of marine carbonate deposits. In the Late Ordovician and Silurian, the amalgamation of the Altyn–Qilian and the South Kunlun Terrane to the south Tarim Basin brought about the subsequent orogeny (Jia, 1997; Yang et al., 1998; Jia and Wei, 2002; Chen and Shi, 2003; Jin et al., 2009; Gao and Fan, 2014). The South Tianshan Ocean to the north of the Tarim Basin was mostly studied to be closed in Carboniferous (Gao et al., 2006). The tectonism in Permian is crucial to the basin evolution: for one thing, the Tianshuihai-Terrace amalgamation close the Tarim Basin forms an intracontinental basin and for the other, the plume beneath the Tarim Basin has strong activities in the Early Permian, forming a large igneous province in the central Tarim basin which was proved by the seismic data, wells, and aeromagnetic data (Yang et al., 1996; Chen et al., 2006; Yang et al., 2013; Li et al., 2014; Xu et al., 2021). The foreland basin dominated the basin Meso–Cenozoic evolution history which has three evolution stages: 1) the Triassic peripheral foreland basin caused by the southward migration and continuous uplift of the Tianshan Mountain (Li et al., 2012); 2) the Jurassic–Paleogene intracontinental depression basin (Zhang et al., 2021), and 3) the Neogene–Quaternary rejuvenated foreland basin due to the collision between the Indian and the Eurasian Plates (Lu et al., 1994; Jia and Wei, 2002; Laborde et al., 2019) (**Figure 2**).

## 2.2 Stratal Units and Tectonic Layers in the Central Tarim Basin

The Tarim Basin is divided into several structural units (**Figure 1A**). The first of these comprises three-fold-thrust belts, including the Kuqa and the Southwest Tarim fold-thrust belts on the margin of the Tarim Block and the Madong fault belt at the central part. Second, four major uplifts are present—the Bachu, the Tazhong, the Tabei, and the East Tarim uplifts. Third, two low uplifts are also located in the area between the Tazhong and the Tabei uplifts, as well as the Manxi and the Gucheng low uplifts in the northern part of the Tazhong uplift and the southeastern part of the Manjiaer Depression (Jia, 1997; Yang et al., 1998; Jia and Wei, 2002). Large and wide strike-slip fault systems have been found in the central Tarim Basin, including the Tabei uplift, the Manxi low uplift, and the Tazhong uplift (**Figure 1A**). Affected by the regional tectonic movements, the Paleozoic can be divided into several regional tectonic layers (**Figure 1B**). Regional extension from the Late Sinian to Mid–Early Cambrian formed rifts, aulacogens, a passive continental margin, and a carbonate platform, where clastic rock, carbonate rock, and evaporite rock deposited. A regional extension to slight compression from the Late Cambrian to Mid–Early Ordovician resulted in weak fault activities and formed a cratonic carbonate platform and slope where dolomite and limestone deposited. Strong regional compression in the Late Ordovician to Silurian formed a series of thrust, uplift, and strike-slip with thick mud rock deposited. From the Devonian to the Carboniferous, cratonic margin depression controlled the marine clastic rock and carbonate rock deposited. In the Permian, due to the intracratonic rift basin and plume, wide volcanic rock formed (Gao and Fan, 2014) (**Figures1B**, **2**, **4**).

## 2.3 Strike-Slip Fault System in the Central Tarim Basin

Large strike-slip fault systems developed from the Tabei uplift to the Tazhong uplift in the central Tarim Basin (**Figure 5**). Several regional strike-slip faults extend from the Tabei uplift to the Tazhong uplift, such as fault $F_I5$, which divided the strike-slip fault systems into two parts. In the east, most strike-slip faults are in the NE–SW orientation; by contrast, the western part of fault $F_I5$ is in the NW–SE trend. The faults in the Tabei uplift are performed like X, diamond, and V shapes, which consists of two sets of faults in the NNE and NNW strike directions (Han et al., 2017; Deng et al., 2019; Wu et al., 2020a). The strike-slip faults in the Tazhong uplift extend in the NE direction in the west part and NEE

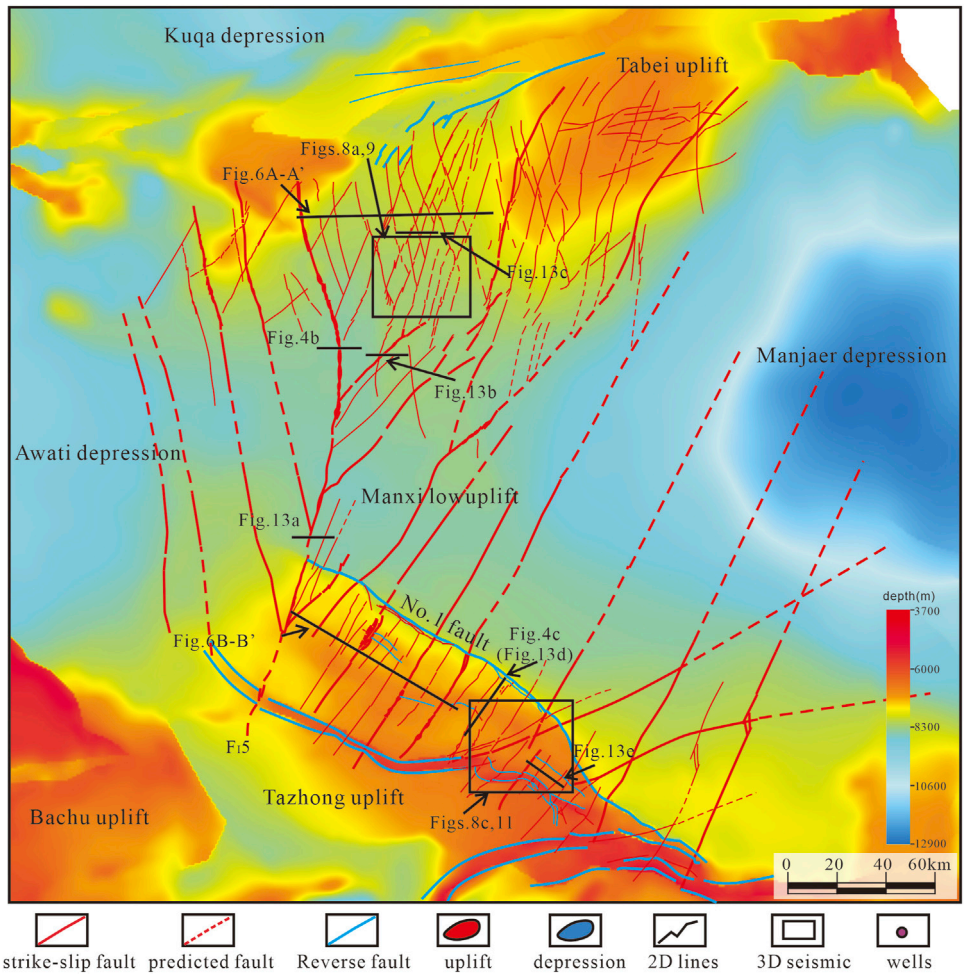


**FIGURE 5 |** Diagram of a strike-slip fault system of the Ordovician carbonate rocks (based on the seismic reflecting surface of the Ordovician Yijianfang Formation, To3).

in the east part, and some of them cut the Tazhong No.1 fault and disappear into the Manjiaer Depression and others ended in the southwest part of the No.1 fault and formed cross and T shapes. In the Manxi low uplift, strike-slip faults connect the Tabei and the Tazhong uplifts, forming Y and V shapes (**Figures 3**, **5**).

## 3 DATA AND METHODS

In this study, three typical 3D seismic surveys over a total area of 15,00 $km^2$ were chosen for comparative research on strike-slip faults in the Tabei uplift and the Tazhong uplift (**Figure 5**), which were obtained from Tarim oilfield company. The 2D/3D seismic data were in post-stack time migration processing and loaded into Halliburton's Landmark Decision Space Geosciences software for interpretation. Several deep wells were used in this area for horizon calibration, which was completed by the Tarim oilfield company. The main seismic reflection surfaces were determined from the Sinian to the Quaternary. They were interpreted carefully (**Figures 4B,C**) such as the bottom of the Sinian (TZ), the bottom of the Cambrian (T$\in$1), the bottom of the Middle Cambrian (T$\in$2), the bottom of the Upper Cambrian (T$\in$3), the bottom of the Ordovician (To1p), the bottom of the Upper Ordovician (To3), the bottom of the Silurian (Ts), the bottom of the Carboniferous (Tc), and the bottom of the Permian (Tp). These reflection surfaces provide lithological information and constrain the interpretation method of strike-slip faults in different layers. In the section view, strike-slip faults can be recognized through the cut-off, bending, or deformation of the main reflectors. Some areas with chaotic seismic reflection configuration also indicated the existence of fault damage zones. A fault-karst reflection was the evidence for secondary faults in the fault belt. Such related structures as reverse faults, grabens, salt tectonics, and volcanic structures were found in special layers, and their relationships with the strike-slip faults were examined. A 3D coherence cube sliced along the reflector surface was used for the 3D interpretation of the strike-slip fault systems in map view (**Figure 4D**).

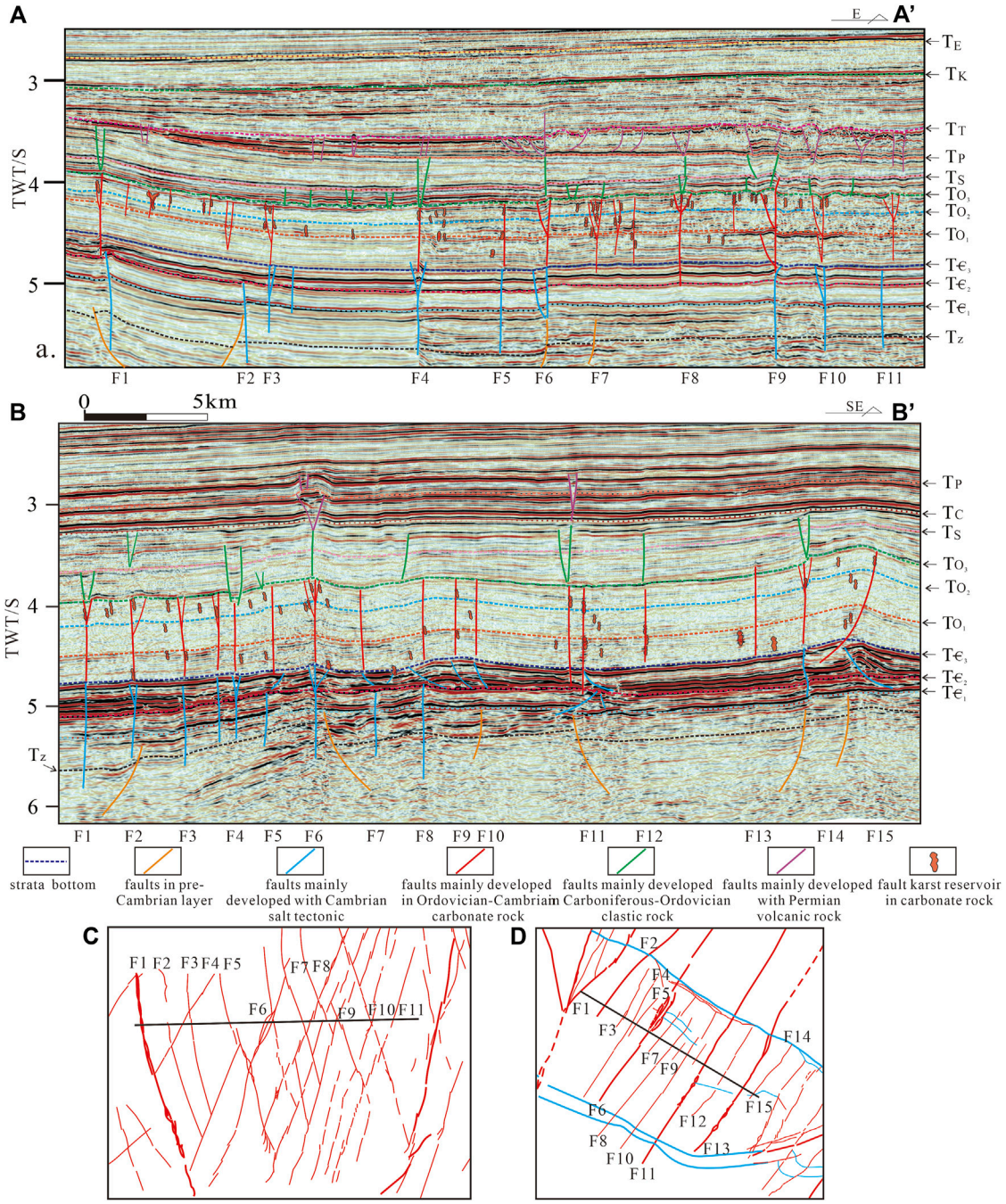


**FIGURE 6 | (A)** Characteristics of layered deformation of typical 3D seismic profiles across strike-slip faults within the Tabei uplift (for location, see **Figure 5**). **(B)** Characteristics of the layered deformation of typical 3D seismic profiles across strike-slip faults within the Tazhong uplift (for location, see **Figure 5**). **(C)** Seismic line location map and fault system of the Tabei uplift. **(D)** Seismic line location map and fault system of the Tazhong uplift. Please refer to the supplementary materials for the uninterpreted seismic data.

Depending on the seismic interpretation, unconformities, growth strata, and fault displacements in different layers were used to determine the evolution stages of strike-slip faults. For example, if positive and negative flower structures were superimposed along the same strike-slip fault in different layers in the section view, it indicated a two-stage evolution history of the given strike-slip fault (**Figures 3C1–C2**).

# 4 CHARACTERISTICS OF STRIKE-SLIP FAULTS IN THE CENTRAL TARIM BASIN

## 4.1 Characteristics of Strike-Slip Fault Deformation Styles in Different Layers

Based on 3D seismic data, deformations in different layers from the Sinian, Cambrian, Ordovician, and Silurian

identified along with the major strike-slip fault system were recognized including reverse faults, normal faults, salt tectonics, and volcanic structures. These findings indicate that strike-slip fault systems occurred due to different tectonic movements and formed mixed structures consisting of various structural styles in different layers (**Figures 4**, **6**).

Strike-slip faults in the Tabei uplift performed various structural styles from the west to the east (**Figures 6A**, **8A**). In the section view, the Ordovician went up to the west owing to tectonic lift; reverse faults (F1 and F2) were found in the western part in the Lower Cambrian superimposed on normal faults in the Sinian in orange (**Figure 6A**). The faults colored in blue, such as F1, were distributed in the Sinian to the Middle Cambrian layer and disappeared in the Middle Cambrian evaporite rock layer (T$\epsilon$2–T$\epsilon$3). The faults exhibited different structures, such as single-fault planes (F5 and F11), V-shaped faults (F4, F6, and F10), positive flower structures (F6, F8, and F9), and negative flower structures (F3 and F10). Some faults in orange located in the Sinian, which cut into the basement, acted like normal faults and influenced faults F1, F2, F6, and F7. Faults F5, F6, and F9 grew upward and were connected to the Ordovician faults, while others were disconnected, such as faults F4, F7, F10, and F11. The strike-slip faults in red from the Upper Cambrian–Ordovician carbonate rock layer occurred as flower structures on top of the carbonate rock layer (To3). Some secondary faults were located between F1 and F3, hanging in the upper part of the Middle Ordovician carbonate layer with some fault-karst reservoirs. Transtension fault in the Silurian (Ts) formed V-type grabens in the clastic rock layer, shown in green, that disappeared upward below the unconformity between the Permian and the Triassic. The Permian became thicker to the east, and the activities of strike-slip fault systems also became stronger, with wider flower structures and longer fault planes than those in the western part. The major faults have some common features. First, the strike-slip fault consists of several deformation layers, from the basement to the Mesozoic. Second, normal faults in the Sinian, reverse faults in the Lower Cambrian, and salt tectonics, such as salt sheets, mini-salt anticlines, and mini-salt sags, in the Middle Cambrian developed with the major strike-slip faults. Third, wider flower structures in the Middle Ordovician carbonate layer influenced the fault-karst reflection distribution. Finally, transtensional faults in the Ordovician–Silurian clastic rocks and fault anticlines in Permian magmatic rock performed various structures styles.

The strike-slip fault system in the Tazhong uplift has stronger layer deformation than that in the Tabei uplift (**Figures 4**, **6B**). In the basement, normal faults controlled the distribution of the Sinian rift system. Some normal faults exhibited strong activities, with the hanging wall thicker than the footwall (F2, F6, F11, and F15), and others performed like transtensional fault systems with a vertical fault plane (F7 and F8). Several faults located in Lower and Middle Cambrian layers, in blue, represent deformation during the Late Cambrian to Mid–Early Ordovician with a slight compression. Some faults had vertical fault planes and cut into the Sinian, while others were gentler and were detached into the Middle Cambrian salt layer. Most faults in this layer ended in the salt layer with strong salt tectonic deformation; for example, salt pillow, salt anticline with detachment thrust, and lens-shaped structures can be recognized through 3D seismic. In the Upper Cambrian–Ordovician carbonate rock layer, strike-slip fault systems were distributed more widely in the west than those in the east. Both negative and positive structures can be found from west to east. In the Upper Ordovician and Silurian clastic rock layers, most faults were transtensional faults and performed V-shape faults or single, vertical faults. In the Permian, most faults stopped; only faults F6 and F11 kept moving upward and formed positive and negative flower structures at the same layer.

Compared with the Tabei uplift, strike-slip faults in the Tazhong uplift exhibited stronger layer deformation, especially in the Sinian and the Lower–Middle Cambrian layer. The following common features were observed. First, basement structures, such as the Silurian rift, influenced the strike-slip fault activities and distribution. Normal faults, reverse faults, and strike-slip faults were found in the Lower and Middle Cambrian layers. Second, salt tectonics played an important role in different deformation styles in the supra-salt layer and subsalt layers. A thick salt layer led to strong varied deformation styles among strike-slip faults. Third, strike-slip faults formed flower structures in different layers that were superimposed vertically (F6); some faults were connected directly (F6, F8, F11, and F14), while others were disconnected or vertically incorrectly positioned (F2, F11, and F15).

## 4.2 Multi-Layer Deformation Models of Strike-Slip Faults

Based on the 3D seismic data interpretation, a total of five deformation layers were identified (**Figure 3A**): a Sinian–Lower Cambrian structural layer (layer 1), a Middle Cambrian salt-related deformation layer (layer 2), a layer of deformed carbonate rocks from the Upper Cambrian to the Middle Ordovician (layer 3), a layer of deformed clastic rocks from the Upper Ordovician to the Carboniferous (layer 4), and a Permian volcanic rock layer (layer 5). Structural styles along the strike-slip faults varied from deep to shallow (**Figure 7**).

Layer 1 represented the subsalt structural layer consisting of a Sinian rift system and reverse faults in the Sinian and the Lower Cambrian. Three types of structural styles were found: normal faults in the Sinian rift system, reverse faults, and paleo-uplifts caused by the tectonic inversion during the Late Cambrian to Mid–Early Ordovician. The seismic data show that strike-slip faults followed the pre-existing fault plane (**Figure 7E1**) or cut through a pre-existing fault (**Figure 7E2**). The paleo-uplift reactivated and induced several strike-slip faults (**Figure 7E3**).

Layer 2 was salt related. The distribution of evaporite rock layers in the Middle Cambrian varied in the central Tarim Basin. A thick salt layer always induced complex deformation styles such as salt sheets, salt anticlines, and complex salt flow structures (**Figure 7D1**). When a strike-slip fault occurred, a thick salt layer caused layered deformation and disconnected fault planes (**Figure 7D3**). When the salt layer became thinner, the strike-slip fault cut through it into the Lower Cambrian (**Figure 7D2**). Three types of structures named salt flow structures, salt sags, and

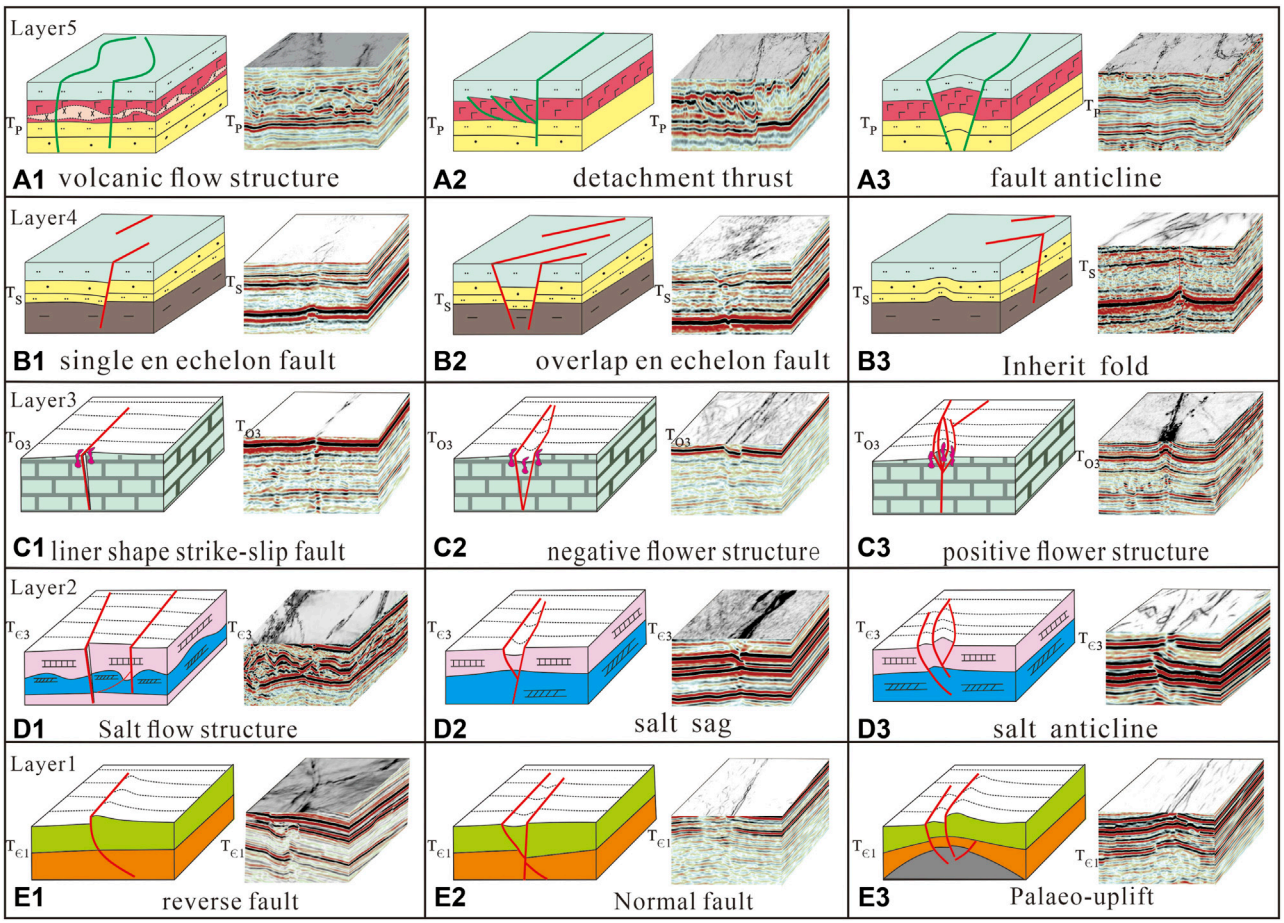


**FIGURE 7 |** Styles of layered deformation of strike-slip fault systems: **(A1–A3)** Permian volcanic rock deformation layer, **(B1–B3)** Upper Ordovician–Silurian clastic rock deformation layer, **(C1–C3)** Upper Cambrian–middle Ordovician carbonate rock deformation layer, **(D1–D3)** Middle Cambrian salt-related deformation layer, and **(E1–E3)** Sinian–Lower Cambrian deformation layer.

salt anticlines represent different tectonic backgrounds when the salt layer deformed (**Figure 7D2**, **D3**).

Layer 3 was an Upper Cambrian–Ordovician carbonate rock layer. On top of the Ordovician carbonate layer, the strike-slip fault had a strong deformation style, such as well-developed flower structures and a wide, straight fault belt (**Figure 7C2**) in the map and section views. Secondary faults mainly developed along major faults and connect to the fault planes at depth to form negative (**Figure 7C2**) and positive (**Figure 7C3**) flower structures. When the strike-slip fault underwent weak transpression or transtension deformation, it performed as a liner shape in map and section view. The fault-karst caves were widely distributed close to the strike-slip faults. These karst caves became smaller from the fault belts to the undeformed rock wall. The fault anticlines and fault blocks always had strong deformation amplitudes, especially in the overlapping zones in map view (**Figure 7C3**).

Layer 4 consisted of the Upper Ordovician mudstones and Silurian clastic rocks. Single en-echelon fault, overlapping en-echelon faults, and inherited folds are three typical styles in this layer. Most strike-slip faults acted like extensional en-echelon faults to form half-grabens (**Figure 7B1**) and grabens (**Figure 7B2**). Inherited folds were found in the Silurian, where the fold formed in the Late Ordovician continued to be activated, and the en-echelon faults were not developed (**Figure 7B3**).

Permian volcanic structures were widely distributed in layer 5 including volcanic flow structures (**Figure 7A1**), detachment thrusts (**Figure 7A2**), and fault anticlines (**Figure 7A3**) which were the three typical structures formed because of the magmatic eruption and intrusion from deep layers along strike-slip faults. Complex deformations were recognized inside the layers and appeared as explosive volcanic facies, effusive facies, and volcano-sedimentary facies that erupted from deep layers into the Permian along strike-slip faults.

## 4.3 Characterization of Strike-Slip Faults in Map View

Strike-slip faults of different structural styles in map view were observed in the central Tarim Basin. These included X-, diamond-, V-, Y-, cross-, and T-shaped faults in deep layers at barrier depths greater than 7,000 m (**Figure 8**). The

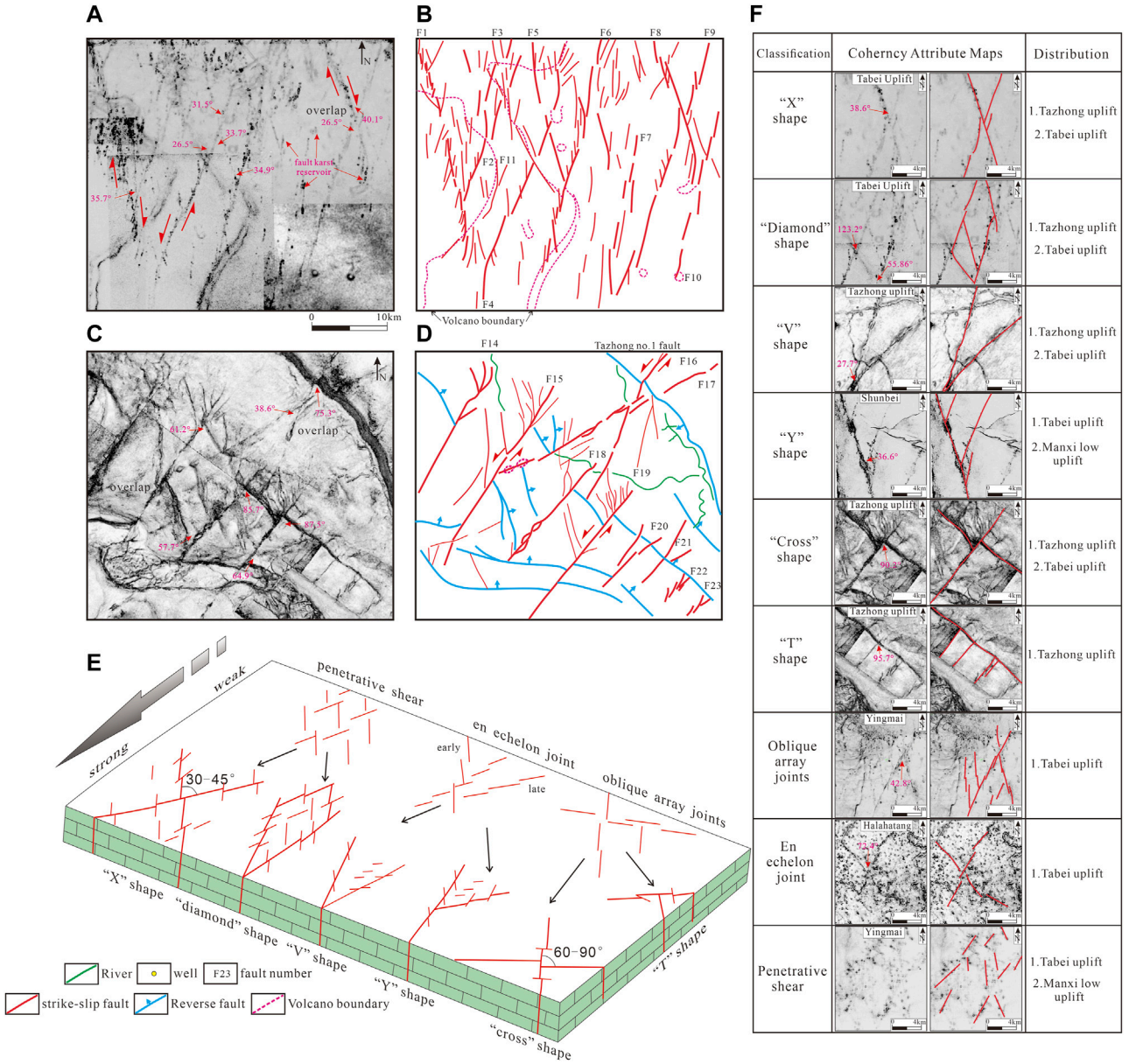


**FIGURE 8 |** Interpretations of strike-slip fault systems from 3D coherence cubes (To3, reflection surface; for location, see **Figure 5**): **(A)** 3D coherence cube slice from the Tabei uplift, **(B)** method of interpreting strike-slip fault systems for the Tabei uplift, **(C)** 3D coherence cube from the Tazhong uplift (for location, see **Figure 5D**, and **(D)** method of interpreting strike-slip fault systems for the Tazhong uplift. **(E)** Models of the strike-slip fault in map view. **(F)** Criteria for fault-type determination used in this study with the corresponding coherency attribute maps.

characteristics of the strike-slip faults in different layers were obtained from 3D seismic coherence slices of Ts, To3, T$\epsilon$3, and T$\epsilon$1 with the seismic lines (**Figures 8–11**) in the Tabei uplift and the Tazhong uplift.

### 4.3.1 Strike-Slip Faults Within the Tabei Uplift

Strike-slip faults were well developed within the Tabei uplift. In this region, severe faults interacted to form a net shape comprising X, V, and diamond shapes. Thus, F5 and F4, as well as F8 and F9, were X-shaped faults, while F3, F4, F2, and F1 were diamond-shaped faults. The X-shaped faults were recognized as conjugate faults (Davis et al., 2000; Wu et al., 2020b). However, the faults, which formed an X shape, performed different activities in different layers (**Figure 9**). The NW trend faults dominated the surfaces of T$\epsilon$1 and TS with the weak activity of NE strike faults (**Figure 9D**). On the surfaces of To3 and T$\epsilon$3, the NE strike faults had longer fault planes than the NW trend faults (**Figures 9B,C**). Some common features were noted. First, fault systems on top of the Ordovician carbonate rocks (To3) did not comprise a single fault but several fault segments.

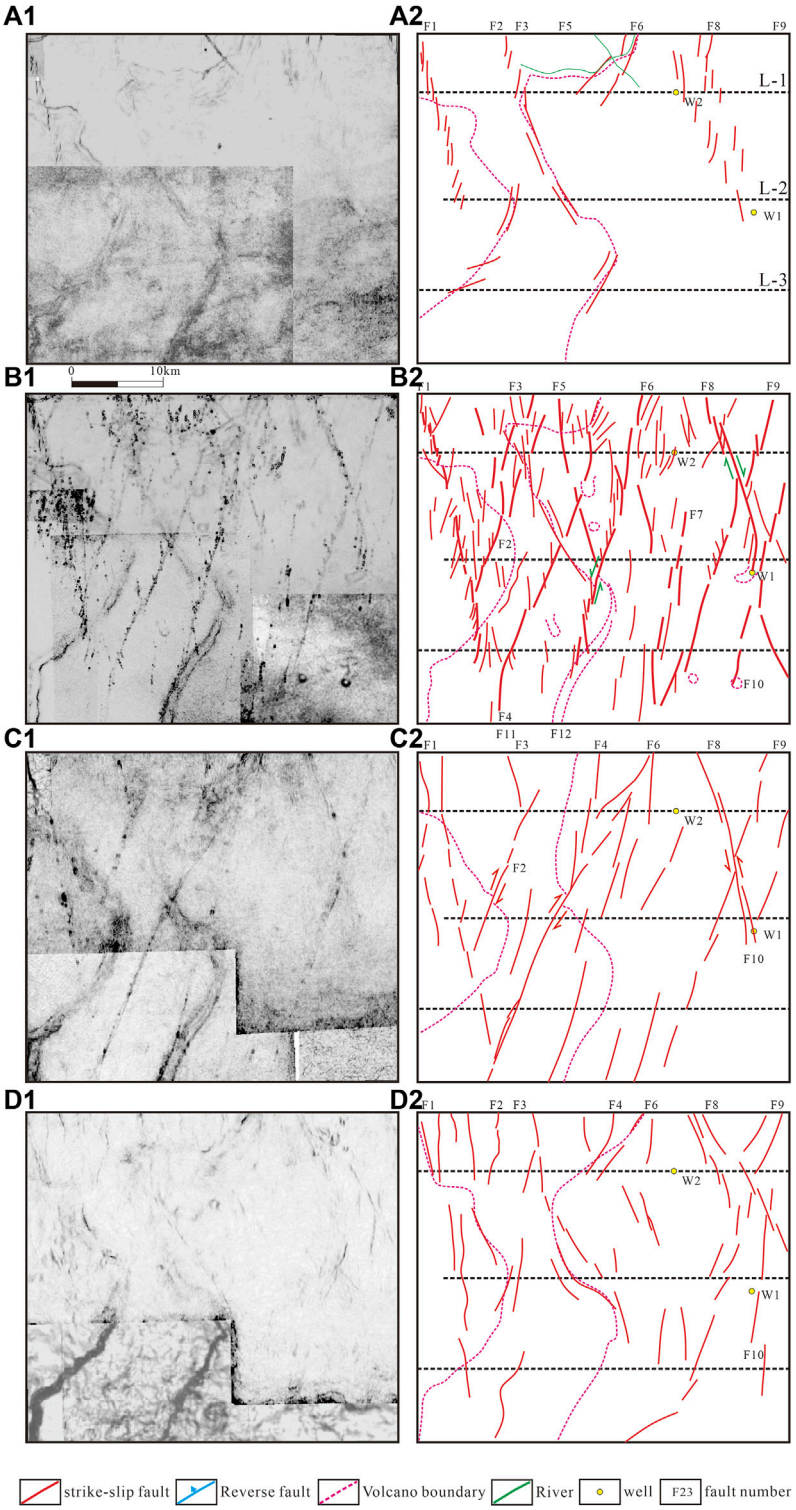


**FIGURE 9 |** Uninterpreted coherence slices (images to the left in **A1–D1**; for location, see **Figure 5**) and interpreted fault systems (images to the right in **A2–D2**) of different seismic reflection surfaces of the Tabei uplift: **(A1)** Ts reflection surface (bottom of the Silurian), **(B1)** To3 reflection surface (bottom of the Upper Ordovician), **(C1)** T$\epsilon$3 reflection surface (bottom of the Upper Cambrian), and **(D1)** T$\epsilon$1 reflection surface (bottom of the Lower Cambrian).

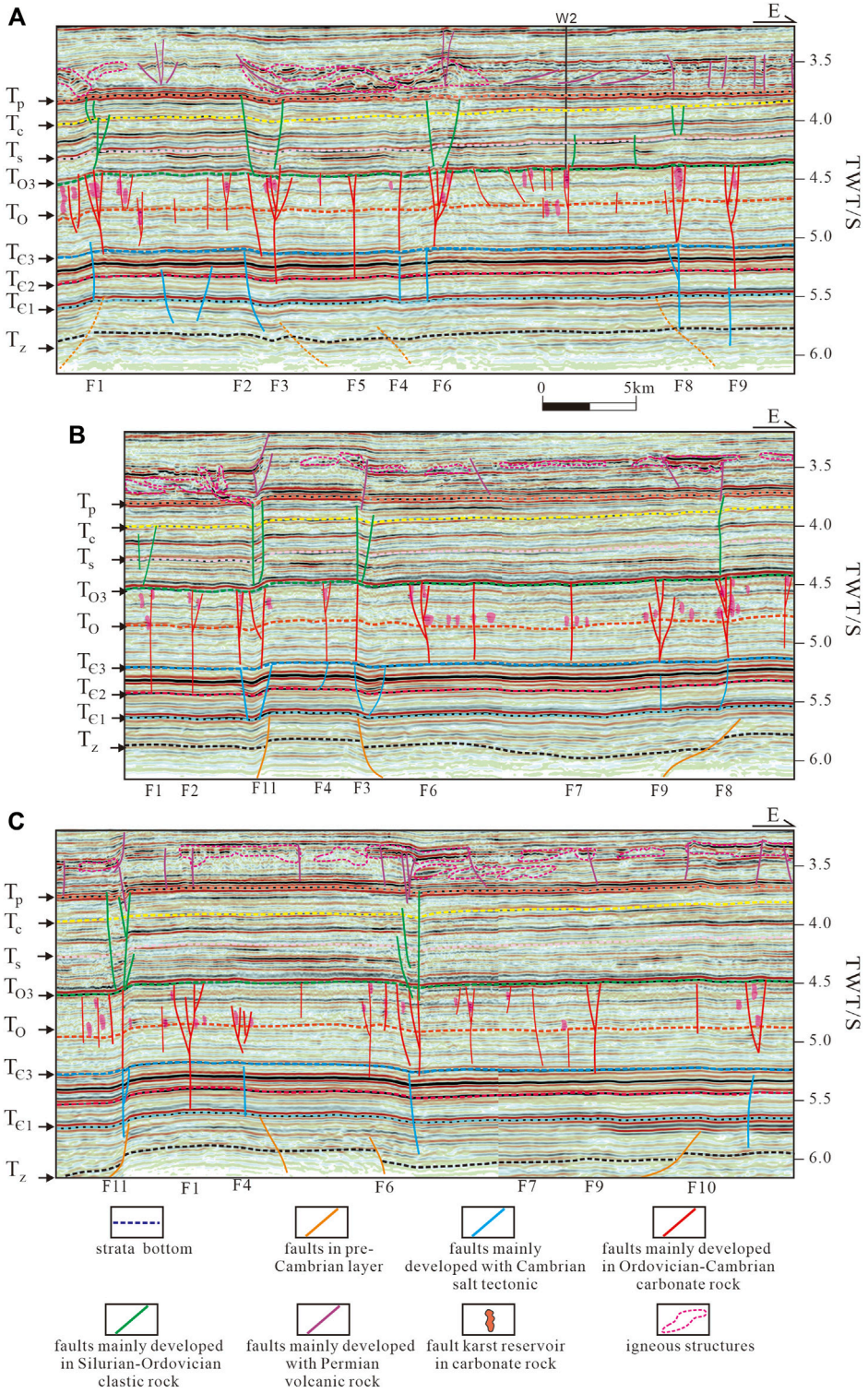


**FIGURE 10 |** 3D seismic profiles of the Tabei uplift (for location, see **Figure 9**): **(A)** 3D seismic line of the northern part (L-1), **(B)** 3D seismic line in the central part (L-2), and **(C)** 3D seismic lines of the southern part (L-3). Please refer to the supplementary materials for the uninterpreted seismic data.

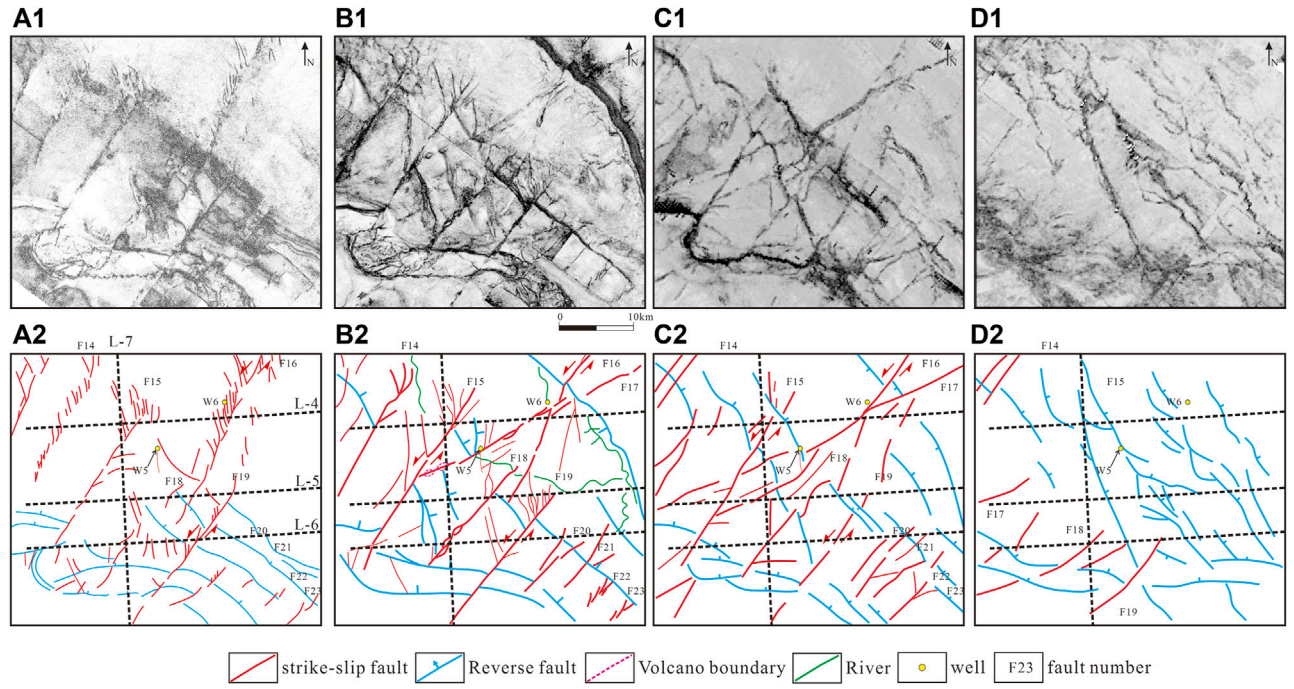


**FIGURE 11 |** Uninterpreted coherence slices (top images in **A1–D1**; for location, see **Figure 5**) and interpreted fault systems (bottom images in **A2–D2**) of different seismic reflection surfaces of the Tazhong uplift: **(A1)** Ts reflection surface (bottom of the Silurian), **(A2)** To3 reflection surface (bottom of the Upper Ordovician), (A3) T$\in$3 reflection surface (bottom of the Upper Cambrian), and (A4) T$\in$1 reflection surface (bottom of the Lower Cambrian).

The fault segments were expressed in en-echelon forms (F8), feather types (F4), and horsetails (F1) (**Figure 9B**). Second, two fault sets were shown to have opposite strike directions and interacted together, including F1 and F4. The first of these, in the west, operated as a right-lateral strike-slip fault (F1) (**Figure 8A**), while its eastern counterpart was expressed as a left-lateral fault (F4). The angles between these sets of faults were measured over a range from 26.5° to 40.1°; thus, faults F8 and F9 formed larger angles in the north and smaller angles in the south. These data show that the fault planes were not straight (**Figure 8A**). Third, the Riedel shear zone was well developed along the major fault, while a left-stepped minor fault array also occurred on the right-lateral strike-slip (F1 and F3) alongside a right-stepped array on the left-lateral strike-slip fault (F6, F4, and F9) (**Figure 8A**). Finally, several secondary faults had occurred inside the blocks between major faults (**Figure 8A**). Some fault-karst reservoirs that appeared round and black in map view and as a beaded reflection in pink in the section view were distributed along with the strike-slip fault system. The density of the fault-karst reservoirs decreased as they moved from the main fault to the secondary faults and the rock wall (**Figures 8A**, **10A**).

The 3D seismic coherence slices show the styles of layered deformation due to the strike-slip faults (**Figure 9**). In the Cambrian subsalt layer (T$\in$1) (**Figure 9D**), most faults had segmented and led to weak deformation, such as left-stepped en-echelon faults or arcuate faults (F1, F3, F8, and F9). Strike-slip faults mainly developed in the NW–SE strike direction; F1, F2, F3, and F8 had clear and longer traces than those in the NE–SW direction, such as F6, F9, and F10. Above the Cambrian salt layer (**Figure 9C**), the strike-slip faults become longer than those in the subsalt layer, two opposite strike-slip fault systems intersected, and some NW–SE strike faults were cut by NE–SW strike faults. For instance, F9 was cut by F8, which indicates that F8 was a left-lateral strike-slip fault. However, on the To3 reflection surface, F8 performed as a right-lateral strike-slip fault (**Figure 9B**). The directions of movement of fault F6 were opposite on the reflection surfaces of T$\in$3 and To3, which verified the strike-slip fault experienced two evolution stages. On the Ts reflection surface, only the NW–SE strike direction faults continued to be activated, forming an en-echelon fault system (**Figure 9A**).

Layered deformation styles were noted through the 3D seismic profiles (**Figure 10**; for location, see **Figure 9**). The faults in the Sinian have weak activities (F1, F5, F4, and F9) with small normal faults, low amplitude sags between F3 and F10, and low uplifts on its west side between F1 and F3. Some faults shown in blue (**Figure 10**) were distributed in the Middle and Lower Cambrian layers that disappeared into the Middle Cambrian layer (F2, F6, F8, and F9). The strike-slip faults were more active in the Ordovician carbonate layer performing wider flower structures, long fault planes (F1, F3, and F4), and bigger fault-karst caves (in pink). With the fault activities decreasing to the south (**Figures 10A–C**), the fault-karst caves become lower and smaller. Some fault-karst caves were distributed inside or along with fault belts, and others were distributed between major faults such as the east side of F6 (**Figure 10B**). The faults in green, distributed in the Silurian–Carboniferous layers, were transtensional fault systems

that acted as normal faults in the seismic profiles. F1, F2, and F6 cut into the Carboniferous and ended in the Permian. Others had weak deformations in the Silurian. From the north (**Figure 10A**) to the south (**Figure 10C**), the fault activities weakened. Permian faults in violet were influenced by volcanic rock. Reverse faults, fault anticlines, and vertical and rotational faults were identified inside the volcanic layer.

### 4.3.2 Strike-Slip Faults in the Tazhong Uplift

A series of cross-shape fault systems had developed in the Tazhong uplift along with the NW–SE striking directional thrusts (**Figure 8D**, blue color) and NE–SW strike-slip fault (red color). First, the angle between the NW–SE fault and the NE–SW faults was larger than that between the X- and Y-shaped faults, between 38.6° and 87.5° (F16, F17, F18, and F19). Second, based on movements of the fault walls, the NE–SW-trend strike-slip fault performed left-lateral movements and cut the NW–SE striking thrusts (F15, F16, and F19). Third, a strike-slip fault also developed like a straight fault plane with a feature type or an en-echelon fault tail (F14, F15, F18, and F19). Secondary faults were influenced by these NW–SE striking thrusts and were formed mainly in the western side of the strike-slip faults (F15, F18, and F19). Fourth, based on the location of these strike-slip faults, three types were identified: boundary, cut, and foot/hanging wall types. The boundary types were located along the transfer zones of the thrusts, such as F18, F15, and F14. By contrast, cut types, including F16, F17, F19, and F20, were formed in the middle part of the thrusts, cut through thrusts, and generated displacements. The foot/hanging wall types were located on the footwall or hanging walls, intersected, or ended on the thrust fault planes, for example, F22 and F23.

The Tazhong uplift had a strong layered deformation style than the Tabei uplift and the Manxi low uplift (**Figure 11**). In the Cambrian subsalt layer, thrusts dominated and performed like the NW-direction trend, dipped to the NE. Strike-slip fault eventually formed in transfer zones between different thrusts in the southwest part of the uplift (**Figure 11D**). The strike-slip faults become longer and stronger in layers above the Cambrian salt layer (**Figure 11C**). Faults F16 and F17 cut the NW strike direction thrust to form a large intersecting angle ranging from 60° to 85°, like cross shaped. The left-lateral strike-slip faults were determined from the movement direction of the cut thrust segments (**Figure 11C**). On the top surface of Ordovician carbonate rocks, the strike-slip faults and thrusts dominate; secondary faults along the major fault formed feather-type, toothbrush-type, braided-type, and small en-echelon faults (**Figure 11B**). On the bottom surface of the Silurian, such faults also performed as right-stepped en-echelon strike-slip faults, varying from the Tabei uplift; most en-echelon faults were developed from linear strike-slip fault planes in the southwest to the en-echelon faults in the northeast (F15, F16, and F19). Thrusts remained active in the southeastern part (F20, F21, F22, and F23).

The stronger layered deformation styles were controlled by the complex evolution history, salt tectonics, and several unconformities (**Figure 12**). Most faults in the subsalt layer performed like reverse faults. Some faults (No. 1 fault, F15, F17, and F19) with thicker hanging walls proved that the faults are normal faults during the Sinian period. Others performed like a strike-slip fault with large flower structures in the subsalt layer. Because of the thick Cambrian salt layer, two fault systems were generated. The detachment thrust above the salt layer and the basement involved thrust in the subsalt layer. F14, F15, and F19 were mainly distributed in the supra-salt layer (**Figure 12**), influenced by the basement thrust faults. Some strike-slip faults were cut into the basement where the thrust fault was not active (F16 and F18). From the north (**Figure 12A**) to the south (**Figure 12C**), the deformation belts of strike-slip faults become narrow, such as F14, F15, and F18. The salt tectonics exhibited as the salt pillows, welt salt rollers, salt anticlines, salt walls, and salt sheets in the Middle Cambrian. The detachment thrusts always detached from the thick salt layer, where the strike-slip faults accompanied the thrusts (F14 and F19) or cut-thrusts (F15). On top of the Ordovician carbonate reflection surface (To3), flower structures were widely distributed. A large deformation belt was observed where the strike-slip fault and thrust intersected, such as in F15 (**Figure 12A**) and F18 (**Figure 12C**). Positive and negative flower structures were found in the same profiles, as in the case of F15 forming positive flower structures and F17 and F19 forming negative flower structures (**Figure 12A**). Some strike-slip faults had opposite activities in different layers, including positive structures in the Cambrian and negative flower structures in the Ordovician. Exemplars include fault F19 (**Figure 12C**), the negative flower structures in the Cambrian, and positive flower structures in the Ordovician, such as F18 (**Figure 12D**). From north to south, the strike-slip faults changed from en-echelon faults to liner-type faults on the bottom surface of the Silurian. The number of faults in the Permian decreased. Only one normal fault and two reverser faults were observed in this area and were superimposed on strike-slip faults F15 and F16 (**Figures 12A–C**). These indicated that the tectonic movement became stronger in the Tabei uplift than in the Tazhong uplift, during the Permian period.

## 4.4 Factors Controlling Deformation Styles of the Strike-Slip Fault

Based on the seismic data interpretation, three factors were found to control the deformation styles of strike-slip faults. They are the multi-stage history of tectonic evolution from the Sinian to the Permian, the lithological combinations from the rift basin to the marine craton basin and rift basin, and the change of regional tectonic stress.

The 3D seismic data show that strike-slip fault belts underwent several deformation stages from the Sinian to the Permian period. In the Sinian deformation layer, sags and paleo-uplifts were recognized below the Cambrian, accompanied by strike-slip faults as a boundary fault in the Manxi low uplift and the Tazhong uplift (**Figures 13A,B,D,E**). The Middle Cambrian salt layer was a key tectonic layer for strike-slip fault deformation. Some transpressional faults, with a high dip angle formed in the Cambrian subsalt layer (**Figures 13A,D**), were distributed wider than the strike-slip faults in the Ordovician layer, which showed that tectonic movement had occurred during Late Cambrian to the Middle–Early Ordovician. Some unconformities with the salt tectonics were

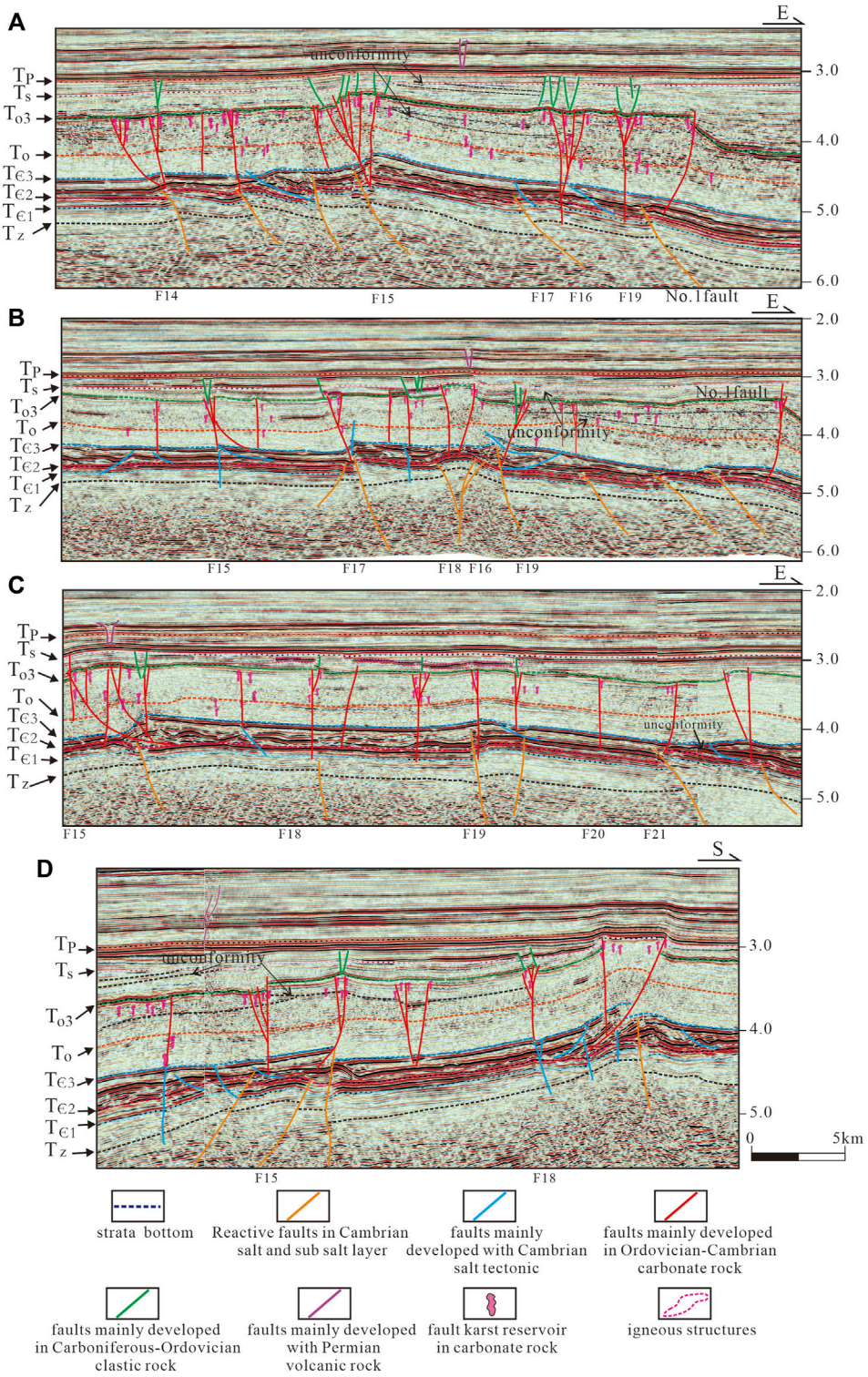


**FIGURE 12 |** 3D seismic profiles of the Tazhong uplift (for location, see **Figure 11**): **(A)** 3D seismic line of the northern part (L-4), **(B)** 3D seismic line of the central part (L-5), **(C)** 3D seismic line of the southern part (L-6), and **(D)** 3D seismic line along an S–N direction (L-7). Please refer to the supplementary materials for the uninterpreted seismic data.

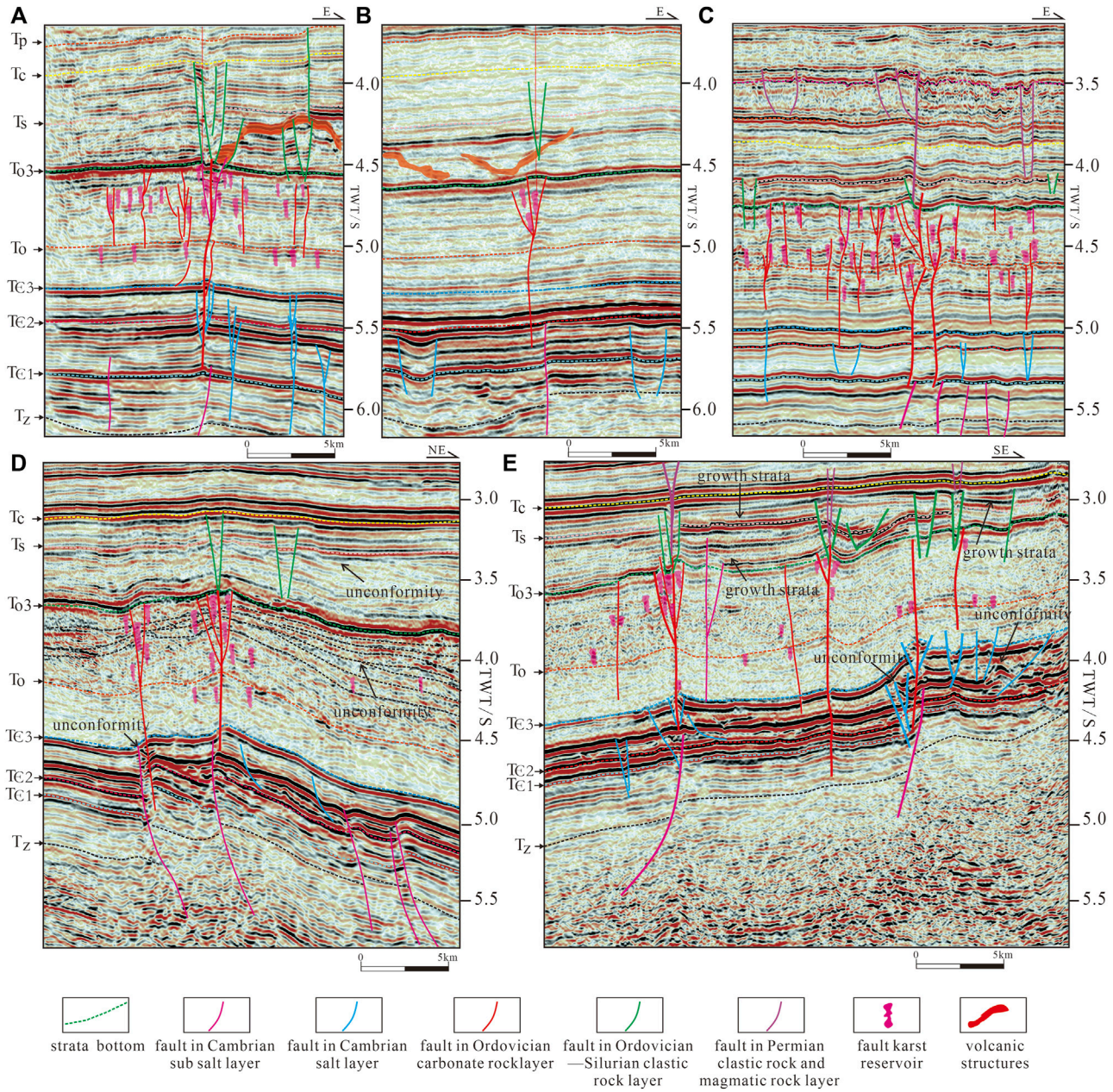


**FIGURE 13 |** 3D seismic profiles of the central Tarim Basin (for location, see **Figure 5**): **(A)** Opposite superposition of strike-slip fault from the Cambrian to the Ordovician in the Manxi low uplift, **(B)** earlier sag in the Cambrian layer in the Manxi low uplift, **(C)** larger fault in the Cambrian layer in the Tabei uplift, **(D)** strong deformation in the Cambrian salt layer and unconformity in the Ordovician layer in the Tazhong uplift, and **(E)** opposite superpositions and strong deformation in the Cambrian salt layer in the Tazhong uplift. Please refer to the supplementary materials for the uninterpreted seismic data.

also found in the Cambrian (**Figures 13D,E**). Because of the change of tectonic stresses from the Late Cambrian to the Middle Ordovician, the flower structures acted like opposite superpositions in different layers, such as the positive follower structures in the Cambrian salt layer and the negative flower structures in the Middle Ordovician layer (**Figures 13A,E**). The displacements of the strike-slip faults decreased from the Cambrian to the Ordovician, indicating that fault activities weakened during different evolution stages (**Figure 13C**). Some folds and fault-karst reflections were recognized above the reflection surface, which indicates that tectonic movements had occurred in the Early Ordovician (**Figures 13B,C,E**). Unconformities (**Figures 13D,E**), volcanic intrusiveness (**Figures 13A,B**), and growth strata (**Figure 13C**) above and below the To3 reflection surface indicated that several tectonic movements had occurred during the Late Ordovician Period. These had induced strong strike-slip fault layered deformations.

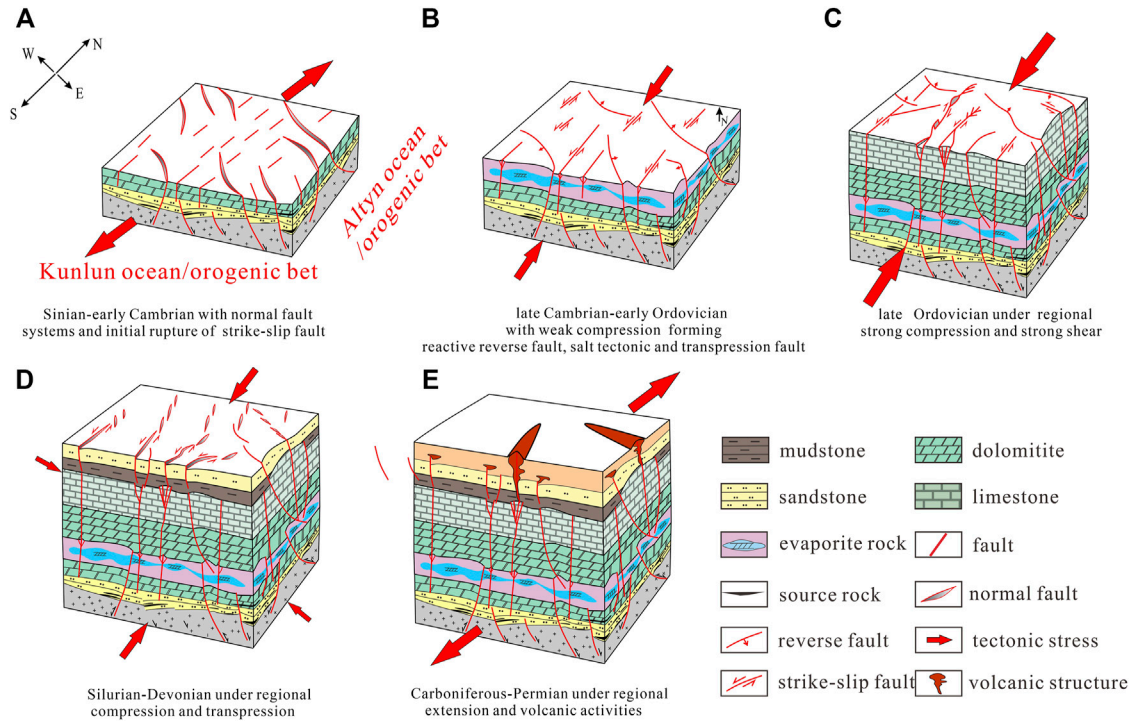


**FIGURE 14 |** Evolution model of the strike-slip fault system of the Tazhong uplift: **(A)** fault evolution stage in the Sinian–Early Cambrian, **(B)** fault evolution stage in the Late Cambrian–Early Ordovician, **(C)** fault evolution stage in the Late Ordovician, **(D)** fault evolution stage in the Silurian–Devonian, and **(E)** fault evolution stage in the Carboniferous–Permian.

The lithological combinations were also a significant factor controlling the styles of the strike-slip faults. When the lithology varied significantly—for example, a transformation from clastic rocks to carbonate or volcanic rocks, from evaporite rocks to dolomite rocks, or carbonate rocks to clastic rocks—flower structures are always generated in the relevant layers. The weak bed like a salt rock layer and mudrock layer could also induce brittleness when the strain rates are high (Davison 2007, 2009) and cause the different fault systems above and below them which also influence the fault types of the strike-slip fault system. Also, a latest study (Bian et al., 2022) regarding the strike-slip salt tectonics in the Tarim Shunbei oilfield has demonstrated that the strike-slip faults in Cambrian weak salt bodies could connect the subsalt source rocks and supra-salt reservoirs, which had imposed significant impacts on petroleum migrations and accumulations.

## 5 DISCUSSION

Former studies have made great achievements in the geometry and kinematics of the strike-slip faults of the Tarim Basin (Jia et al., 1998; Han et al., 2017; Wu et al., 2018; Neng et al., 2018; Deng et al., 2019; Wu et al., 2020a; Wu et al., 2020b), while their conclusions are not consistent. The research on the relationship between strike-slip fault and other tectonics is still insufficient, especially in the Cambrian and Permian evolution stage.

A key period of tectonic change refers to a period when the basin dynamic characteristics and sedimentary environments change greatly which influenced not only the thrust faults and salt tectonics but also strike-slip faults. In this study, the regional stress fields of different periods that responded to periphery plate tectonic movements were mainly concluded from previous research (Jia et al., 1998; Wu et al., 2018; Qiu et al., 2019; Deng, et al., 2021; Qiu et al., 2022). The evolution model of the strike-slip faults was built to associate strike-slip fault evolution with the regional stress field alternations (**Figures 14**, **15**).

Previous studies show that the Tarim Basin experienced several tectonic cycles and the regional tectonic stress changed several times (Jia and Wei, 2002; Liu and Wang, 2012). In the Early Sinian, most of the Tarim Basin was repeatedly uplifted with some small rift basin and aulacogen in the northeastern and western part of the Tarim Basin under the extension stress field (refer to Tian, et al., 2020 and Bai et al., 2020 for the location of the rift). In the late Sinian, the Tarim Basin became a cratonic depression. At this stage, Manjiaer depression and Awati depressions were cratonic marginal basins (Jia and Wei, 2002). The normal faults and grabens dominated this tectonic layer. Influenced by the Kuluktak-Manjiaer aulacogen, the Tabei and Tazhong area had more normal faults in the eastern part than in the western part (**Figures 14A**, **15A**). During the Early–Middle Cambrian, the central Tarim experienced an extensional tectonic background with a

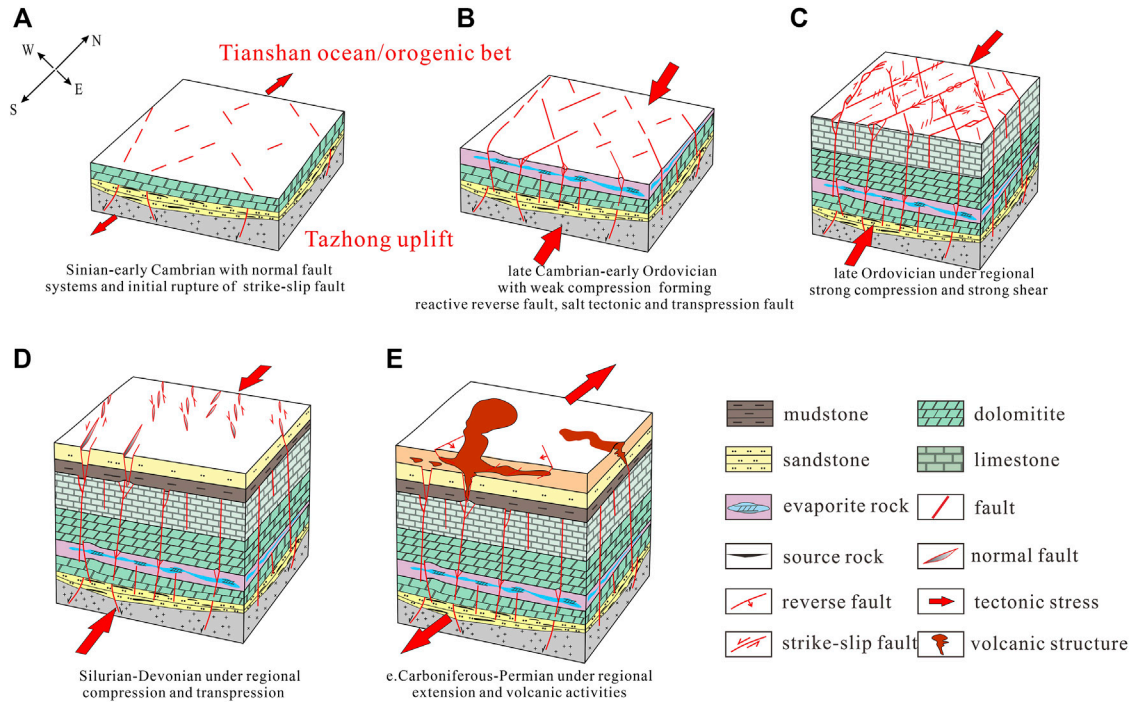


**FIGURE 15 |** Evolution model of the strike-slip fault system of the Tabei uplift: **(A)** fault evolution stage in the Sinian–Early Cambrian, **(B)** fault evolution stage in the Late Cambrian–Early Ordovician, **(C)** fault evolution stage in the Late Ordovician, **(D)** fault evolution stage in the Silurian–Devonian, and **(E)** fault evolution stage in the Carboniferous–Permian.

passive continental margin developed in the southwest and northeast, followed by a short episode of weak localized compression which lead to the compressive-reverse movements and foldings after the Early–Middle Cambrian (Gao and Fan, 2014). Some pre-existing faults were reactivated, and initial rupture of the strike-slip fault formed (**Figures 14A**, **15A**). From the Late Cambrian to the Middle Ordovician, the ocean basins surrounding the Tarim Basin evolved dramatically: The north Tianshan Ocean began to subduct southwards beneath the Central Tianshan Microcontinent, generating compressive stress to the South, and the North Kunlun Ocean subducted to the North forming compressive stress (Jia and Wei 2002; Gao and Fan, 2014). These compressive stresses formed the initial strike-slip faults and reverse faults, foldings, and salt tectonics in the central Tarim Basin. The fault activities in the Tazhong area were stronger than those of the Tabei area during this period (**Figures 14B**, **15B**). In the latest Middle Ordovician, regional compression strengthened and the Tarim craton became an active continental margin. The southwest Tarim, Tabei, and Tazhong areas uplifted. In the Late Ordovician, thrust faults formed accompanied with strike-slip faults. The thrust activities weakened from south to north as a result of the Kunlun, Altun ocean closure, and orogenies in the southern part of the Tarim craton (Gao and Fan, 2014). Fault segments were connected to form kinds of fault patterns along the fault belt. The thrusts formed together with the strike-slip faults, which also had stronger activities in the Tazhong uplift than in the Tabei uplift. The X, V, diamond type formed in the Tabei uplift, while the T and cross type formed in the Tazhong area (**Figures 14C**, **15C**). During the Silurian–Devonian, Late Caledonian movements, and Hercynian movements caused the collision between the Tarim block and the Central Tianshan–Yining block. Also, the South Tianshan narrow ocean transformed into a foreland basin. Transtension en-echelon faults formed in this time, which weakened from the south Tazhong uplift to the north Tabei uplift (**Figures 14D**, **15D**). From the Carboniferous to the early stage of the Permian Period, the southern margin of the Tarim continental plate was a passive continental margin, which became an active continental margin in the late stage of the Early Permian–Late Permian when the Paleo–Tethys closed to the south of the Tarim continental plate and triggered the isle arc volcanic activity. The northern margin of the Tarim Basin was an active continental margin, as the oblique collision between the Tarim continental plate and the Middle Tianshan block occurred. The igneous activity of the intracratonic rift of the Tarim Basin occurred in the Early Permian. The volcanic activity in the Tabei uplift was stronger and more complex than that of the Tazhong uplift (**Figures 14E**, **15E**). In this study, the strike-slip fault deformation and fault patterns in the Sinian, the Early–Middle Cambrian, and the Permian were addressed and associated with the regional tectonic evolution studies (Jia et al., 1998; Li et al., 2007; Han et al., 2017; Neng et al., 2018; Wu et al., 2018; Deng et al., 2019; Wu et al., 2020a; Wu et al., 2020b), which was not systemically documented in previous studies.

## 6 CONCLUSION

A large strike-slip fault system was widely distributed in the Paleozoic layer of the central Tarim Basin, which formed X-, V-, Y-, diamond-, cross-, and T-shaped deformation styles on the top of the Ordovician carbonate layer. The X-, V-, and diamond-shaped deformation styles were mainly observed in the Tabei uplift, and the cross- and T-shaped deformation styles dominated the Tazhong uplift.

The strike-slip fault system consists of a five-layered architecture. They are normal faults and transtensional faults in the Sinian and reverse, transtensional, and transpressional faults with salt tectonics in the Lower–Middle Cambrian. Wider flower structures and fault-karst were found in the Ordovician carbonate rock layer. The en-echelon transtension system mainly developed from the Late Ordovician to the Carboniferous. Volcanic structures along the strike-slip fault formed thrusts, normal faults, and folds in the Permian.

The multi-stage tectonic evolution history from the Sinian to Permian, lithological combinations from the rift basin to the marine basin, and regional tectonic stresses were the main factors influencing layered deformation structural styles. The evolution history of the strike-slip fault started from the earlier Cambrian and ended in the Mesozoic.

## DATA AVAILABILITY STATEMENT

The original contributions presented in the study are included in the article/**Supplementary Material**; further inquiries can be directed to the corresponding authors.

## AUTHOR CONTRIBUTIONS

YN: conceptualization, project administration, writing—original draft, writing—review and editing, and funding acquisition. YL: resources and supervision. JQ: organization, supervision, and methodology. XM: conceptualization, investigation, software, Writing—review & editing. LZ: formal analysis. PC: investigation.

## FUNDING

This work was supported by the Xinjiang Uighur Autonomous Region Tianshan Talent Project and Xinjiang Uighur Autonomous Region University Scientific Research Project, Number XJEDU 2019Y072.

## ACKNOWLEDGMENTS

The authors are grateful for constructive comments and suggestion from three reviewers. This work was supported by the Xinjiang Uygur Autonomous Region Natural Science Foundation Research Project (2021D01A199) as well as by a Xinjiang Uygur Autonomous Region Department of Education College Scientific Research project (XJEDU 2019Y072).

## SUPPLEMENTARY MATERIAL

The Supplementary Material for this article can be found online at: https://www.frontiersin.org/articles/10.3389/feart.2022.837354/full#supplementary-material

## REFERENCES

Aydin, A., and Berryman, J. G. (2010). Analysis of the Growth of Strike-Slip Faults Using Effective Medium Theory. *J. Struct. Geol.* 32 11, 1629–1642. doi:10.1016/j.jsg.2009.11.007

Bai, Z., Cheng, M., and Chen, C. (2020). Distribution Features of the Nanhua-Sinian Rifts and Their Significance to Hydrocarbon Accumulation in the Tarim Basin. *Acta Geol. Sin. Engl. Ed.* 94, 15. doi:10.1111/1755-6724.14340

Basile, C., and Brun, J. P. (1999). Transtensional Faulting Patterns Ranging from Pull-Apart Basins to Transform Continental Margins: an Experimental Investigation. *J. Struct. Geol.* 21, 23–37. doi:10.1016/s0191-8141(98)00094-7

Berglar, K., Gaedicke, C., Franke, D., Ladage, S., Klingelhoefer, F., and Djajadihardja, Y. S. (2010). Structural Evolution and Strike-Slip Tectonics off North-Western Sumatra. *Tectonophysics* 480 (1-4), 119–132. doi:10.1016/j.tecto.2009.10.003

Bian, Q., Deng, S., Lin, H., and Han, J. (2022). Strike-slip Salt Tectonics in the Shuntuoguole Low Uplift, Tarim Basin, and the Significance to Petroleum Exploration. *Mar. Petroleum Geol.* 139, 105600. doi:10.1016/j.marpetgeo.2022.105600

Carroll, A. R., Graham, S. A., Hendrix, M. S., Ying, D., and Zhou, D. (1995). Late Paleozoic Tectonic Amalgamation of Northwestern China: Sedimentary Record of the Northern Tarim, Northwestern Turpan, and Southern Junggar Basins. *Geol. Soc. Am. Bull.* 107, 571–594. doi:10.1130/0016-7606(1995)107<0571:lptaon>2.3.co;2

Chen, H. L., Yang, S. F., Wang, Q. H., Luo, J. C., Jia, C. Z., Wei, G. Q., et al. (2006). Sedimentary Response to the Early-MidPermian Basaltic Magmatism in the Tarim Plate. *Geol. China* 33, 545. doi:10.3969/j.issn.1000-3657.2006.03.010

Chen, Z. Q., and Shi, G. R. (2003). Late Paleozoic Depositional History of the Tarim Basin, Northwest China: An Integration of Biostratigraphic and Lithostratigraphic Constraints. *Bulletin* 87, 1323–1354. doi:10.1306/0401032001115

Cunningham, W. D., Windley, B. F., Dorjnamjaa, D., Badamgarov, J., and Saandar, M. (1996). Late Cenozoic Transpression in Southwestern Mongolia and the Gobi Altai-Tien Shan Connection. *Earth Planet. Sci. Lett.* 140, 67–81. doi:10.1016/0012-821x(96)00048-9

Davis, G. H., Bump, A. P., Garcı´a, P. E., and Ahlgren, S. G. (2000). Conjugate Riedel Deformation Band Shear Zones. *J. Struct. Geol.* 22, 169–190. doi:10.1016/s0191-8141(99)00140-6

Davison, I. (2009). Faulting and Fluid Flow through Salt. *J. Geol. Soc.* 166, 205–216. doi:10.1144/0016-76492008-064

Davison, I. (2007). "*Geology and Tectonics of the South Atlantic Brazilian Salt Basins*,". Editors A. C. Ries, R. W. H. Butler, and R. H. Graham (London: Geological Society, Special Publication), 272, 345–359. doi:10.1144/gsl.sp.2007.272.01.18

Deng, S., Liu, Y., Liu, J., Han, J., Wang, B., and Zhao, R. (2021). Structural Styles and Evolution Models of Intracratonic Strike-Slip Faults and the Implications for Reservoir Exploration and Appraisal: A Case Study of the Shunbei Area, Tarim Basin. *Geotect. Metallogenia* 45 (6), 1111–1126.

Deng, S., Li, H., Zhang, Z., Zhang, J., and Yang, X. (2019). Structural Characterization of Intracratonic Strike-Slip Faults in the Central Tarim Basin. *Bulletin* 103, 109–137. doi:10.1306/06071817354

Deng, S., Zhao, R., Kong, Q., Li, Y., and Li, B. (2022). Two Distinct Strike-Slip Fault Networks in the Shunbei Area and its Surroundings, Tarim Basin: Hydrocarbon Accumulation, Distribution, and Controlling Factors. *Bulletin* 106 (1), 77–102. doi:10.1306/07202119113

Dooley, T. P., and Schreurs, G. (2012). Analogue Modelling of Intraplate Strike-Slip Tectonics: a Review and New Experimental Results. *Tectonophysics* 574-575, 1–71. doi:10.1016/j.tecto.2012.05.030

Faulkner, D., Lewis, A., and Rutter, E. (2003). On the Internal Structure and Mechanics of Large Strike-Slip Fault Zones: Field Observations of the Carboneras Fault in Southeastern Spain. *Tectonophysics* 367 (3–4), 235–251. doi:10.1016/s0040-1951(03)00134-3

Gao, J., Long, L., Qian, Q., Huang, D., Su, W., and Reiner, K. (2006). South Tianshan: A Late Paleozoic or a Triassic Orogen? *Acta Petrol. Sin.* 22 (5), 1049. doi:10.3321/j.issn:1000-0569.2006.05.001

Gao, Z., and Fan, T. (2014). Intra-platform Tectono-Sedimentary Response to Geodynamic Transition along the Margin of the Tarim Basin, NW China. *J. Asian Earth Sci.* 96, 178–193. doi:10.1016/j.jseaes.2014.08.023

Haijun, Y., Chen, Y., Tian, J., Du, J., Zhu, Y., Li, H., et al. (2020). Great Discovery and its Significance of Ultra-deep Oil and Gas Exploration in Well Luntan1 of the Tarim Basin. *China Pet. Explor.* 25, 62. doi:10.3969/j.issn.1672-7703.2020.02.007

Han, X., Deng, S., Tang, L., and Cao, Z. (2017). Geometry, Kinematics and Displacement Characteristics of Strike-Slip Faults in the Northern Slope of Tazhong Uplift in Tarim Basin: A Study Based on 3D Seismic Data. *Mar. Petroleum Geol.* 88, 410–427. doi:10.1016/j.marpetgeo.2017.08.033

Harding, T. P. (1974). Petroleum Traps Associated with Wrench Faults. *Am. Assoc. Petroleum Geol. Bull.* 58 (7), 1290–1304. doi:10.1306/83d91669-16c7-11d7-8645000102c1865d

Jia, C., and Wei, G. (2002). Structural Characteristics and Petroliferous Features of Tarim Basin. *Chin. Sci. Bull.* 47, 1–11. doi:10.1007/bf02902812

Jia, C. Z. (1997). Tectonic Characteristics and Petroleum, Tarim Basin. *China. Pet. Ind. Press*, 1–120. (in Chinese with English abstract).

Jia, D., Lu, H., Cai, D., Wu, S., Shi, Y., and Chen, S. (1998). Structural Features of Northern Tarim Basin: Implications for Regional Tectonics and Petroleum Traps. *AAPG Bull.* 82, 147–159. doi:10.1306/1d9bc3b3-172d-11d7-8645000102c1865d

Jin, Z., Zhu, D., Hu, W., Zhang, X., Zhang, J., and Song, Y. (2009). Mesogenetic Dissolution of the Middle Ordovician Limestone in the Tahe Oilfield of Tarim Basin, NW China. *Mar. Petroleum Geol.* 26, 753–763. doi:10.1016/j.marpetgeo.2008.08.005

Laborde, A., Barrier, L., Simoes, M., Li, H., Coudroy, T., Van der Woerd, J., et al. (2019). Cenozoic Deformation of the Tarim Basin and Surrounding Ranges (Xinjiang, China): A Regional Overview. *Earth-Science Rev.* 197, 102891. doi:10.1016/j.earscirev.2019.102891

Li, C., Wang, X., Li, B., and He, D. (2013a). Paleozoic Fault Systems of the Tazhong Uplift, Tarim Basin, China. *Mar. Petroleum Geol.* 39, 48–58. doi:10.1016/j.marpetgeo.2012.09.010

Li, D., Yang, S., Chen, H., Cheng, X., Li, K., Jin, X., et al. (2014). Late Carboniferous Crustal Uplift of the Tarim Plate and its Constraints on the Evolution of the Early Permian Tarim Large Igneous Province. *Lithos* 204, 36–46. doi:10.1016/j.lithos.2014.05.023

Li, Y., Yang, H., Zhang, G., Zheng, D., Liu, Y., Zhao, Y., et al. (2012). Redivision of the Tectonic Units of Tabei Rise in Tarim Basin, NW China. *Acta Petrol. Sin.* 28 (8), 2466

Lin, B., Zhang, X., Xu, X., Yuan, J., Neng, Y., and Zhu, J. (2015). Features and Effects of Basement Faults on Deposition in the Tarim Basin. *Earth-Science Rev.* 145, 43–55. doi:10.1016/j.earscirev.2015.02.008

Little, T. A. (1995). Brittle Deformation Adjacent to the Awatere Strike-Slip Fault in New Zealand: Faulting Patterns, Scaling Relationships, and Displacement Partitioning. *Geol. Soc. Am. Bull.* 107 (11), 1255–1271. doi:10.1130/0016-7606(1995)107<1255:bdatta>2.3.co;2

Liu, H., and Wang, Y. (2012). Restoration of Eroded Stratal Thickness in Key Periods of Tectonic Change in a Multi-Stage Superimposed Tarim Basin in China. *J. Palaeogeogr.* 1, 149. doi:10.3724/SP.J.1261.2012.00012

Lu, H. F., Howell, D. G., Jia, D., and Al, E. (1994). Rejuvenation of the Kuqa Foreland Basin, North Flank of Tarim Basin, Northwest China. *Int. Geol. Rev.* 36, 1151

Lu, X., Wang, Y., Tian, F., Li, X., Yang, D., Li, T., et al. (2017). New Insights into the Carbonate Karstic Fault System and Reservoir Formation in the Southern Tahe Area of the Tarim Basin. *Mar. Petroleum Geol.* 86, 587–605. doi:10.1016/j.marpetgeo.2017.06.023

Mathieu, L., and van Wyk de Vries, B. (2011). The Impact of Strike-Slip, Transtensional and Transpressional Fault Zones on Volcanoes. Part 1: Scaled Experiments. *J. Struct. Geol.* 33 (5), 907–917. doi:10.1016/j.jsg.2011.03.002

McClay, K. R., and Bonora, M. (2001). Analog Models of Restraining Stepovers in Strike-Slip Fault Systems. *AAPG Bull.* 85, 233–260. doi:10.1306/8626c7ad-173b-11d7-8645000102c1865d

Morley, C. K. (2002). A Tectonic Model for the Tertiary Evolution of Strike-Slip Faults and Rift Basins in SE Asia. *Tectonophysics* 347, 189–215. doi:10.1016/s0040-1951(02)00061-6

Neng, Y., Wu, G., Huang, S., Zhang, X., and Cao, S. (2016). Formation Stage and Controlling Factors of the Paleo-Uplifts in the Tarim Basin: A Further Discussion. *Nat. Gas. Ind. B* 3, 209–215. doi:10.1016/j.ngib.2016.05.005

Neng, Y., Xie, H., Yin, H., Li, Y., and Wang, W. (2018). Effect of Basement Structure and Salt Tectonics on Deformation Styles along Strike: An Example from the Kuqa Fold-Thrust Belt, West China. *Tectonophysics* 730, 114–131. doi:10.1016/j.tecto.2018.02.006

Neng, Y., Yang, H., and Deng, X. (2018). Structural Patterns of Fault Damage Zones in Carbonate Rocks and Their Influences on Petroleum Accumulation in Tazhong Paleo-Uplift, Tarim Basin, NW China. *Petroleum Explor. Dev.* 45, 43–54. doi:10.1016/s1876-3804(18)30004-1

Nicholson, C., Seeber, L., Williams, P., and Sykes, L. R. (1986). Seismic Evidence for Conjugate Slip and Block Rotation within the San Andreas Fault System, Southern California. *Tectonics* 5, 629–648. doi:10.1029/tc005i004p00629

Nur, A., Ron, H., and Scotti, O. (1986). Fault Mechanics and the Kinematics of Block Rotations. *Geology* 14 (9), 746–749. doi:10.1130/0091-7613(1986)14<746:fmatko>2.0.co;2

Pang, H., Chen, J., Pang, X., Liu, L., Liu, K., and Xiang, C. (2013). Key Factors Controlling Hydrocarbon Accumulations in Ordovician Carbonate Reservoirs in the Tazhong Area, Tarim Basin, Western China. *Mar. Petroleum Geol.* 43, 88–101. doi:10.1016/j.marpetgeo.2013.03.002

Pluhar, C. J., Coe, R. S., Lewis, J. C., Monastero, F. C., and Glen, J. (2006). Fault Block Kinematics at a Releasing Stepover of the Eastern California Shear Zone: Partitioning of Rotation Style in and Around the Coso Geothermal Area and Nascent Metamorphic Core Complex. *Earth Planet. Sci. Let.* 250 1–2, 134–163. doi:10.1016/j.epsl.2006.07.034

Qiu, H., Deng, S., Cao, Z., Yin, T., and Zhang, Z. (2019). The Evolution of the Complex Anticlinal Belt with Crosscutting Strike-Slip Faults in the Central Tarim Basin, NW China. *Tectonics* 38 (6), 2087–2113. doi:10.1029/2018tc005229

Qiu, H., Deng, S., Zhang, J., Lin, H., Huang, C., Han, J., et al. (2022). The Evolution of a Strike-Slip Fault Network in the Guchengxu High, Tarim Basin (NW China). *Mar. Petroleum Geol.* 140, 105655. doi:10.1016/j.marpetgeo.2022.105655

Rolland, Y., Alexeiev, D. V., Kröner, A., Corsini, M., Loury, C., and Monié, P. (2013). Late Palaeozoic to Mesozoic Kinematic History of the Talas-Ferghana Strike-Slip Fault (Kyrgyz West Tianshan) as Revealed by 40ar/39ar Dating of Syn-Kinematic White Mica. *J. Asian Earth Sci.* 67-68 (may), 76–92. doi:10.1016/j.jseaes.2013.02.012

Shen, W., Chen, J., Wang, Y., Zhang, K., Chen, Z., Luo, G., et al. (2019). The Origin, Migration and Accumulation of the Ordovician Gas in the Tazhong III Region, Tarim Basin, NW China. *Mar. Petroleum Geol.* 101, 55–77. doi:10.1016/j.marpetgeo.2018.11.031

Storti, F., Holdsworth, R. E., and Salvini, F. (2003). "Intraplate Strike-Slip Deformation Belts," in *Intraplate Strike-Slip Deformation Belts* (London: Geological Society, London, Special Publications), 210, 1–14. doi:10.1144/gsl.sp.2003.210.01.01

Sutton, J., and Watson, J. V. (1986). *Architecture of the Continental Lithosphere*, 317. London, Series A: Philosopical Transactions of the Royal Society, 5

Sylvester, A. G. (1988). Strike-Slip Faults. *Geol. Soc. Am. Bul.* 100 (11), 1666–1703. doi:10.1130/0016-7606(1988)100<1666:SSF>2.3.CO;2

Tian, Lei., Zhang, H., and Liu, J. (2020). Distribution of Nanhua-Sinian Rifts and Proto-type Basin Evolution in Southwestern Tarim Basin, NW China[J]. *Petroleum Explor. Dev.* 47, 62–73. doi:10.1016/s1876-3804(20)60130-1

Turner, S. A. (2010). Sedimentary Record of Late Neoproterozoic Rifting in the NW Tarim Basin, China. *Precambrian Res.* 181, 85–96. doi:10.1016/j.precamres.2010.05.015

Wang, Z., Gao, Z., Fan, T., Shang, Y., Qi, L., and Yun, L. (2020). Structural Characterization and Hydrocarbon Prediction for the SB5M Strike-Slip Fault Zone in the Shuntuo Low Uplift, Tarim Basin. *Mar. Petroleum Geol.* 117, 104418. doi:10.1016/j.marpetgeo.2020.104418

Woodcock, N. H., and Fischer, M. (1986). Strike-Slip Duplexes. *J. struct. geol.* 8 7, 725–735. doi:10.1016/0191-8141(86)90021-0

Wu, G., Kim, Y.-S., Su, Z., Yang, P., Ma, D., and Zheng, D. (2020a). Segment Interaction and Linkage Evolution in a Conjugate Strike-Slip Fault System from the Tarim Basin, NW China. *Mar. Petroleum Geol.* 112, 104054. doi:10.1016/j.marpetgeo.2019.104054

Wu, G., Yang, S., Meert, J. G., Xiao, Y., Chen, Y., Wang, Z., et al. (2020b). Two Phases of Paleoproterozoic Orogenesis in the Tarim Craton: Implications for Columbia Assembly. *Gondwana Res.* 83, 201–216. doi:10.1016/j.gr.2020.02.009

Wu, G., Zhao, K., Qu, H., Scarselli, N., Zhang, Y., Han, J., et al. (2020c). Permeability Distribution and Scaling in Multi-Stages Carbonate Damage Zones: Insight from Strike-Slip Fault Zones in the Tarim Basin, NW China. *Mar. Petroleum Geol.* 114, 104208. doi:10.1016/j.marpetgeo.2019.104208

Wu, L., Guan, S., Zhang, S., Yang, H., Jin, J., Zhang, X., et al. (2018). Neoproterozoic Stratigraphic Framework of the Tarim Craton in NW China: Implications for Rift Evolution. *J. Asian Earth Sci.* 158, 240–252. doi:10.1016/j.jseaes.2018.03.003

Xu, X., Zuza, A. V., Yin, A., Lin, X., Chen, H., and Yang, S. (2021). Permian Plume-Strengthened Tarim Lithosphere Controls the Cenozoic Deformation Pattern of the Himalayan-Tibetan Orogen. *Geology* 49 (1), 96–100. doi:10.1130/g47961.1

Yang, S., Chen, H., Li, Z., Li, Y., Yu, X., Li, D., et al. (2013). Early Permian Tarim Large Igneous Province in Northwest China. *Sci. China Earth Sci.* 56, 2015–2026. doi:10.1007/s11430-013-4653-y

Yang, S. F., Chen, H. L., Dong, C. W., Jia, C. Z., and Wang, Z. G. (1996). The Discovery of Permiansyenite inside Tarim Basin and its Geodynamic Significance. *Geochimica* 25, 121–128. [in Chinese].

Yang, S. F., Chen, H. L., Dong, C. W., Zhao, D. D., Jia, C. Z., and Wei, G. Q. (1998). Geochemical Properties of Late Sinian Basalt in the Northwestern Boundary of Tarim Basin and its Tectonic Setting. *J. Zhejiang Univ. Nat. Sci.)* 32, 753–760. (in Chinese with English abstract).

Yu, J., Li, Z., Li, Z., and Yang, L. (2016). Fault System Impact on Paleokarst Distribution in the Ordovician Yingshan Formation in the Central Tarim Basin, Northwest China. *Mar. Petroleum Geol.* 71, 105–118. doi:10.1016/j.marpetgeo.2015.12.016

Yu, Y., Tang, L., Yang, W., Huang, T., Qiu, N., and Li, W. (2014). Salt Structures and Hydrocarbon Accumulations in the Tarim Basin, Northwest China. *Bulletin* 98, 135–159. doi:10.1306/05301311156

Yuzhu, K., and Zhihong, K. (1996). Tectonic Evolution and Oil and Gas of Tarim Basin. *J. Southeast Asian Earth Sci.* 13, 317–325. doi:10.1016/0743-9547(96)00038-4

Zhang, Z., Lin, C., Liu, Y., Zhao, H., Li, H., Sun, Q., et al. (2021). Lacustrine to Fluvial Depositional Systems: The Depositional Evolution of an Intracontinental Depression and Controlling Factors, Lower Cretaceous, Northern Tarim Basin, Northwest China[J]. *Mar. Petroleum Geol.* 126, 104904. doi:10.1016/j.marpetgeo.2021.104904

Zhiqian, G., and Tailiang, F. (2015). Unconformities and Their Influence on Lower Paleozoic Petroleum Reservoir Development in the Tarim Basin. *J. Petroleum Sci. Eng.* 133, 335–351. doi:10.1016/j.petrol.2015.06.015

Zhu, G.-Y., Ren, R., Chen, F.-R., Li, T.-T., and Chen, Y.-Q. (2017). Neoproterozoic Rift Basins and Their Control on the Development of Hydrocarbon Source Rocks in the Tarim Basin, NW China. *J. Asian Earth Sci.* 150, 63–72. doi:10.1016/j.jseaes.2017.09.018

Zouaghi, T., Bédir, M., and Inoubli, M. H. (2005). 2d Seismic Interpretation of Strike-Slip Faulting, Salt Tectonics, and Cretaceous Unconformities, Atlas Mountains, Central tunisia. *J. Afr. Earth Sci.* 43 (4), 464–486. doi:10.1016/j.jafrearsci.2005.09.010

**Conflict of Interest:** The author YL was employed by Research Institute of Petroleum Exploration and Development, Tarim Oilfield Company, PetroChina.

The remaining authors declare that the research was conducted in the absence of any commercial or financial relationships that could be construed as a potential conflict of interest.

**Publisher's Note:** All claims expressed in this article are solely those of the authors and do not necessarily represent those of their affiliated organizations, or those of the publisher, the editors, and the reviewers. Any product that may be evaluated in this article, or claim that may be made by its manufacturer, is not guaranteed or endorsed by the publisher.